iScience

Article

A developmental atlas of mouse vestibular-like inner ear organoids

Graphical abstract

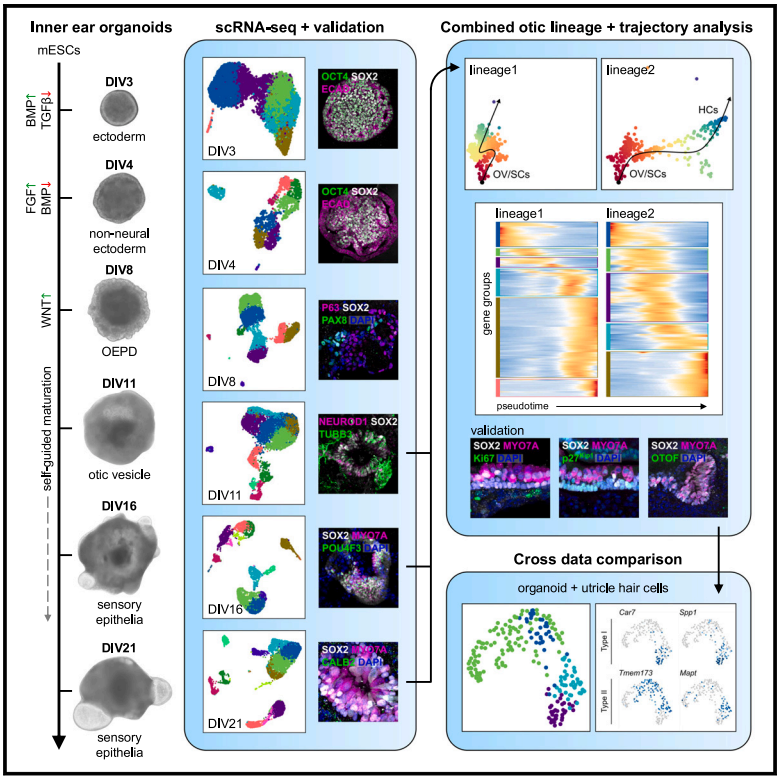

Highlights

- We use scRNA-seq to study inner ear epithelia development in mESC-derived organoids
- Otic lineage commitment in organoids mirrors key steps of mouse development
- Organoid-derived sensory epithelia shift from high proliferation to a non-proliferative state
- Organoid hair cells are immature at the time of supporting cell quiescence

Authors

Maggie S. Matern, Stefan Heller

Correspondence

mmatern@stanford.edu

In brief

Stem cells research; Developmental biology; Transcriptomics

Matern & Heller, 2025, iScience *28*, 111817
February 21, 2025
https://doi.org/10.1016/j.isci.2025.111817

CellPress

iScience

CellPress
OPEN ACCESS

Article

A developmental atlas of mouse vestibular-like inner ear organoids

Maggie S. Matern[1,2,3,*] and Stefan Heller[1,2]
[1]Department of Otolaryngology — Head and Neck Surgery, Stanford University School of Medicine, Stanford, CA 94304, USA
[2]Institute for Stem Cell Biology & Regenerative Medicine, Stanford University School of Medicine, Stanford, CA 94304, USA
[3]Lead contact
*Correspondence: mmatern@stanford.edu
https://doi.org/10.1016/j.isci.2025.111817

SUMMARY

Inner ear sensory epithelia can be generated *in vitro* from embryonic stem cells. The resulting inner ear organoids represent a potentially inexhaustible source of otic tissues, including sensory hair cells and supporting cells, for *in vitro* manipulation. Here, we present a single-cell atlas of whole mouse embryonic stem cell-derived vestibular-like inner ear organoids at six developmental stages. Our analyses trace the genesis and developmental progression of otic progenitor cells to supporting cells and hair cells. By profiling all organoid cells, we also characterize the development of additional cell groups, such as otic mesenchyme. We further utilize our atlas to describe a proliferative phase where otic progenitors produce hair cells and otic neuroblasts, followed by a transition to a non-proliferative state. The resulting map of otic progression reveals specific time windows that can inform future research on cell cycle regulation and cell lineage specification in inner ear organoids.

INTRODUCTION

Many head sensory organs originate from cranial sensory placodes that are specified during early embryonic development. These placodes, or ectodermal thickenings on the embryo's surface, are induced by exposures to varying levels of morphogenic factors such as BMPs, WNTs, and FGFs.[1] In recent years, researchers have exploited the spatiotemporal activity of signaling factors and developmental morphogens during embryogenesis to guide stem cells *in vitro* through ectoderm formation and into specific cell types.[2] These *in vitro* models typically result in three-dimensional cell clusters that bear organ-specific organoids, which are scalable and quickly manipulatable alternatives to using *in vivo* animal models.

Organoid models are especially valuable for generating rare tissue and cell types, such as the sensory epithelia of the inner ear.[3] Using successive exposures to BMP, FGF, and WNT, combined with modulation of TGFβ signaling, DeJonge et al.[3] developed a protocol to induce the formation of otic lineage cells in an organoid system (Figure 1A). Like organoids for other organ models,[2] these inner ear organoids represent a potentially limitless source of tissue for studying the development, function, and response of inner ear tissues to ototoxic and regenerative drugs.[4] A current limitation of stem cell guidance protocols toward otic induction is that existing protocols generate potentially generic inner ear cells, lacking complete specification of vestibular or cochlear traits. However, recent advances suggest that it might be possible to overcome these limitations in the future.[5]

Here, our goal was to provide more insight into inner ear cell lineage development within the reliable and extensively validated mouse embryonic stem cell (mESC)-derived vestibular-like inner ear organoid protocol.[3,6–9] We used single-cell RNA-sequencing (scRNA-seq) to investigate the steps of otic placode induction and inner ear sensory epithelia formation within the organoid environment. In total, we profiled 34,823 cells from six organoid formation time points, subjected them to computational identification, and utilized them to assess transcriptional dynamics during sensory lineage progression. By generating this atlas, we found that otic organoid development progressed through the postulated stages of ectoderm, non-neural ectoderm, otic epibranchial progenitor domain, otic vesicle, and sensory epithelia formation. Additionally, by profiling whole organoids, we have defined co-developing cell types, such as epidermis, muscle, otic mesenchyme, and otic neurons. Surprisingly, we observed simultaneous hair cell and otic neuroblast formation within otic vesicle-like structures as early as 11 days following initiation of the protocol; a phenomenon that does not exist in the developing *in vivo* inner ear. Furthermore, a pseudotime trajectory analysis of developing sensory epithelia from our three most advanced organoid time points revealed robust proliferation of otic vesicle-like structures before transitioning into generic supporting cells and vestibular-like hair cells.

Overall, our organoid developmental atlas represents a useful resource for studying the interplay between co-developing cell types within inner ear organoids. Our studies further highlight the usefulness of inner ear organoids as a simplified model for studying and manipulating the development of specific cell types, such as hair cells.

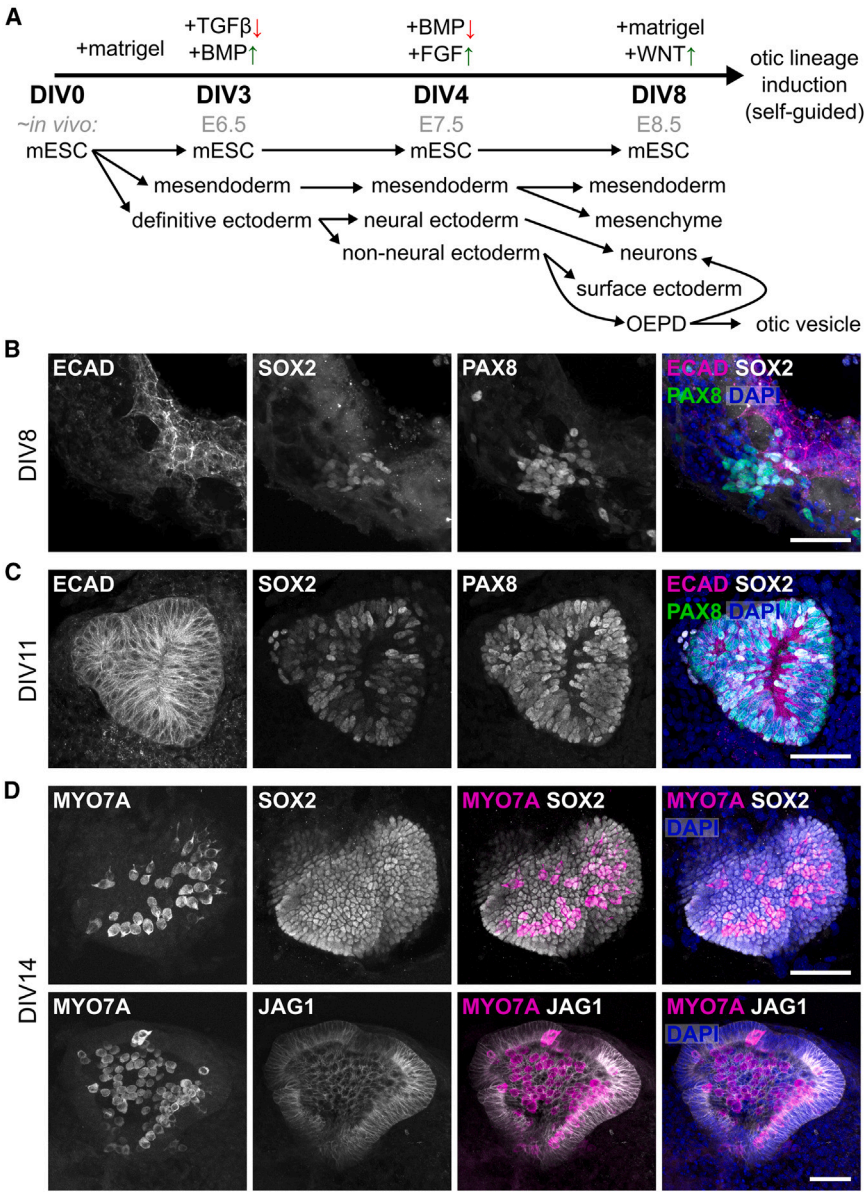

Figure 1. Modulation of TGFβ, BMP, FGF, and WNT signaling results in the formation of inner ear sensory epithelia *in vitro*

(A) Overview of the mouse embryonic stem cell (mESC)-derived inner ear organoid protocol. DIV, days *in vitro*; ↓, inhibition; ↑, activation; OEPD, otic epibranchial progenitor domain.

(B) By DIV8, non-neural ectoderm gives rise to ECAD+/SOX2+/PAX8+ OEPD.

(C) By DIV11, OEPD cells further differentiate to form ECAD+/SOX2+/PAX8+ otic vesicle structures.

(D) By DIV14, otic vesicle structures mature into sensory epithelia, complete with SOX2+/JAG1+ supporting cells and MYO7A + hair cells. Scale = 50 μm, $n \geq 3$.

RESULTS

Rapid generation of ectoderm, non-neural ectoderm, and pre-placodal ectoderm in early developing mESC-derived inner ear organoids

mESC-derived inner ear organoids were generated following the protocol outlined in DeJonge et al., 2016, which results in detectable vestibular-like sensory epithelial cell types at 14 days *in vitro* (DIV14) (Figures 1A–1D). Whole organoids were collected and dissociated for 10x Genomics scRNA-seq at DIV3, 4, 8, 11, 16, and 21. At DIV3, 72 h after mESC aggregation in floating culture and 48 h after the addition of 2% matrigel, our data revealed four distinct cell populations distributed into six clusters. The cell populations represented *Sox2*+/*Nanog*+ mESCs (Figures 2A and 2B, Data S1, DIV3 cluster 1, 27.7%), transitioning mESCs that are upregulating ectoderm/neural ectoderm markers such as *Nes* (DIV3 cluster 3, 19.4%), and presumed ectoderm/neural ectoderm cells that express higher levels of *Cdh1* and *Nes*, as well as the neural ectoderm markers *Pou3f1* and *Tubb3* (DIV3 clusters 2, 4, and 5, 52.2%).[10–12] Additionally, we identified a small population of *Gata6*+/*Sox17*+/*Pdgfra*+ mesendoderm cells (DIV3 cluster 6, 0.8%).[13]

BMP4 and a TGFβ signaling inhibitor were added to the organoid culture media at DIV3 to bias the formation of non-neural ectoderm over neural ectoderm. 24 hours (h) later, at DIV4, scRNA-seq revealed a substantial transition to *Gata3*+/*Tfap2a*+ non-neural ectoderm (Figures 2C and 2D, Data S1, DIV4 clusters 1, 2, 3, and 5, 62.7%).[14] Conversely, the remaining ectoderm was reduced to a smaller population of *Cdh2*+/*Pou3f1*+ neural ectoderm (DIV4 clusters 6 and 7, 20.4%).[8] Additionally, compared to DIV3, a shrinking population of *Nanog*+/*Sox2*+ mESCs (DIV4 cluster 4, 11.1%) and a growing population of *Gata6*+/*Sox17*+ mesendoderm cells (DIV4 cluster 9, 1.7%) were identified. qPCR validation of selected population marker gene expression indeed revealed a rapid reduction of *Nanog* and *Sox2* expression between DIV0 (mESCs) and DIV3, as well as an increase in *Pdgfra* and *Sox17* expression by DIV4, indicative of a reduction of mESC-specific gene expression and upregulation of markers for specific lineages within the developing organoids (Figure 2E). This is confirmed at the protein level as a reduction of mESC markers SOX2 and OCT4 at the ECAD-positive outer edges of organoids between DIV3 and DIV4 (Figure 2F). Validation of ectoderm and neural ectoderm markers by qPCR revealed a repression of *Nes* and *Pou3f1* between DIV3 and DIV4, while *Cdh2* is maintained (Figures 2B, 2D, and 2E). According to our scRNA-seq results, *Nes* and *Pou3f1* are initially more widely expressed

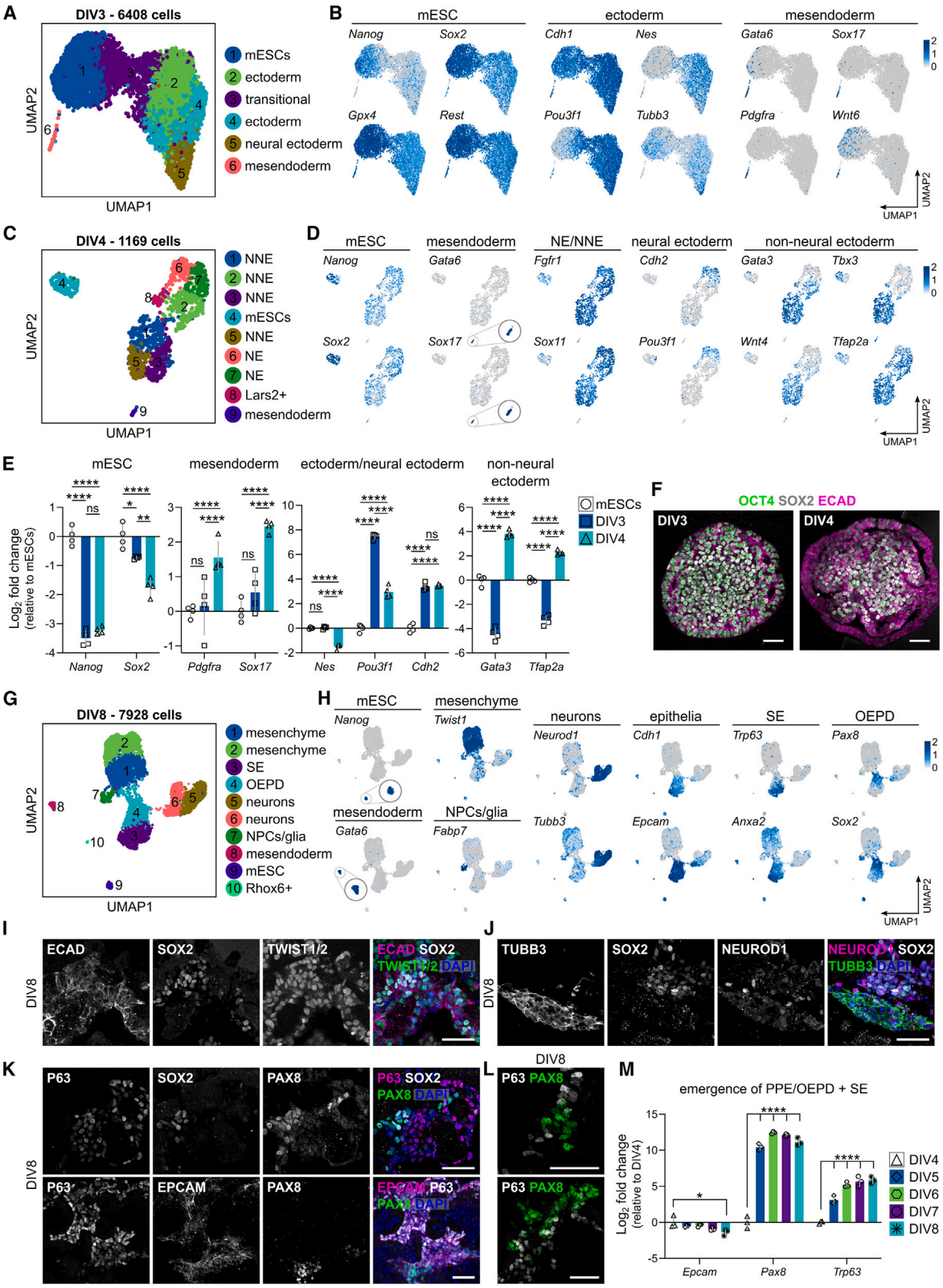

(legend on next page)

in the presumed ectoderm at DIV3 and then either fully repressed (*Nes*) or restricted to non-neural ectoderm (*Pou3f1*) by DIV4 (Figure S1). This likely reflects the rapid action of BMP signaling to induce non-neural ectoderm over neural ectoderm. In support of this, qPCR validation of non-neural ectoderm markers revealed an initial repression of *Tfap2a* and *Gata3* between DIV0 (mESCs) and DIV3 which was followed by a rapid and robust upregulation between DIV3 and DIV4 (Figure 2E). The initial downregulation of non-neural ectoderm markers may reflect ambient RNA expression by mESCs, which have been shown to express many lineage-specific genes while maintaining pluripotency.[15]

At DIV4, FGF2 was added to the culture media along with a BMP inhibitor to induce the transition of non-neural ectoderm to pre-placodal ectoderm (PPE) followed by the induction of otic epibranchial progenitor domain cells (OEPD) by DIV8.[8] Clustering of our scRNA-seq data of whole organoids at DIV8 revealed a small group of *Nanog*+ mESCs (Figures 2G and 2H, Data S1, DIV8 cluster 9, 1.5%), *Gata6*+ mesendoderm cells (DIV8 cluster 8, 1.8%), a small population of *Sox2*+/*Fabp7*+ neural precursor cells (NPCs)/glia (DIV8 cluster 7, 2.8%), large populations of *Twist1*+ mesenchymal cells (DIV8 clusters 1 and 2, 45.7%, Figure 2I), and *Neurod1*+/*Tubb3*+ neurons (DIV8 clusters 5 and 6, 19.4%, Figure 2J).[16–18] The remaining cells, representing 28.5% of all organoid cells, expressed epithelial markers *Cdh1* and *Epcam* (Figure 2H). These cells consisted of two distinct populations, one corresponding to developing surface ectoderm (SE) based on the expression of epidermal markers *Trp63* and *Anxa2* (DIV8 cluster 3, 15.2%), and the other group representing OEPD cells based on the expression of *Sox2* and *Pax8* (DIV8 cluster 4, 13.3%).[8,17] Immunohistochemistry revealed that EPCAM+/PAX8+/SOX2+ OEPD cells are located adjacent to EPCAM+/P63+ SE cells (Figure 2K). The expression of PAX8 and P63 does not appear to overlap (Figures 2K and 2L), suggesting distinct commitment of placodal and surface ectodermal lineages at DIV8. To further pinpoint the timing of PPE and SE development, we utilized qPCR to assess the induction of the *Pax8* and *Trp63* after FGF2 and BMP inhibitor exposure at DIV4. While the overall epithelial composition of organoids remains stable up to DIV7 based on *Epcam* expression, there is significant induction of both *Pax8* and *Trp63* between DIV4 and DIV5 (Figure 2M), suggesting a rapid transition of non-neural ectoderm to PPE and SE after FGF2 and BMP inhibitor exposure. This reveals an interesting opportunity to modulate PPE versus SE development within organoids at DIV4, and highlights the utility of our emerging single-cell atlas for identifying such time points for protocol modification.

Simultaneous otic neuroblast and hair cell development within otic vesicle-like structures at DIV11

At DIV8, the culture conditions of developing organoids were transitioned to maturation media containing 1% matrigel and the Wnt activator CHIR99021. This change in the signaling environment has been previously shown to induce the formation of otic vesicle cells.[3] Subsequent scRNA-seq at DIV11 revealed an increase in the proportion of *Twist1*+ mesenchymal cells (Figures 3A and 3B, Data S1, DIV11 clusters 1–5, 76.7%). A subset of these mesenchymal cells also expressed the otic mesenchyme marker *Pou3f4* (clusters 3 and 4, 20.1%).[19] Within DIV11 organoids, POU3F4+ cells are present adjacent to ECAD+/SOX2+ otic vesicle-like structures but are also mixed with presumed POU4F3- mesenchymal cells (Figure 3C). Our DIV11 data also revealed a sustained population of *Gata6*+/*Sox17*+ mesendoderm (DIV11 cluster 9, 2.0%).

With respect to neuronal and epithelial cell subgroups, we identified *Neurod1*+/*Tubb3*+ neurons (DIV11 cluster 6, 8.1%), as well as *Epcam*+/*Trp63*+/*Krt5*+ epidermal cells (DIV11 clusters 8 and 10, 7.3%) and *Epcam*+/*Trpm3*+/*Jag1*+/*Sox2*+ otic vesicle cells (DIV11 cluster 7, 5.9%).[17,20,21] Similar to DIV8, PAX8+/JAG1+ otic vesicle structures were observed near a layer of P63+ epidermis (Figure 3D). This arrangement is reminiscent of the invagination of otic-fated cells from the developing surface ectoderm during embryogenesis, although otic morphogenesis in organoids in general is not well organized.[22]

While validating the neuronal population in DIV11 organoids, we observed that SOX2+ otic vesicle structures also contained NEUROD1+ and TUBB3+ cells (Figure 3E). A few NEUROD1+ cells co-labelled for SOX2 (Figure 3F) and TUBB3+ cells were EPCAM+ (Figures 3G and 3H). We hypothesized that these TUBB3+ cells represent a population of delaminating otic neuroblasts, similar to those seen in the ventral neurosensory competent domain of the otic vesicle during embryonic

Figure 2. scRNA-seq of DIV3, DIV4 and DIV8 inner ear organoids

(A and B) scRNA-seq of DIV3 organoids reveals the transition of mESCs to ectoderm and neural ectoderm, as well as a small population of mesendoderm, as demonstrated by select marker gene expression.

(C and D) scRNA-seq of DIV4 organoids reveals the further transition of ectoderm to non-neural ectoderm, as demonstrated by select marker gene expression. See also Figure S1.

(E) qPCR validation of differential gene expression between mESCs, DIV3, and DIV4 organoids, $n = 4$. p value *<0.05, **<0.01, ****<0.0001, ns = not significant. Significance was assessed by two-way ANOVA followed by Tukey's multiple comparisons test. Data are represented as mean ± SD.

(F) Immunostaining for the pluripotency markers OCT4 and SOX2 reveals the specification of an outer layer of OCT4-/SOX2-/ECAD+ ectoderm lineage cells at DIV4. Scale, 50 μm, $n \geq 3$.

(G and H) scRNA-seq of DIV8 organoids shows the formation of *Sox2*+/*Pax8*+ otic-epibranchial progenitor domain cells (OEPD), in addition to mesenchyme, neural precursor cells (NPCs)/glia, neurons, and surface ectoderm (SE).

(I and J) Validation of TWIST1/2+/ECAD-SOX2- mesenchymal cells and TUBB3+ neurons at DIV8.

(K and L) EPCAM+/SOX2+/PAX8+ OEPD and EPCAM+/P63+ SE develop adjacently but do not overlap. Scale = 50μm, $n \geq 3$.

(M) While the overall level of *Epcam* expression does not change between DIV4 and DIV7, *Pax8* and *Trp63* are rapidly induced between DIV4 and DIV5. PPE, pre-placodal ectoderm; $n = 3$.

p value *<0.05, ****<0.0001. Significance was assessed by two-way ANOVA followed by Tukey's multiple comparisons test. Data are represented as mean ± SD.

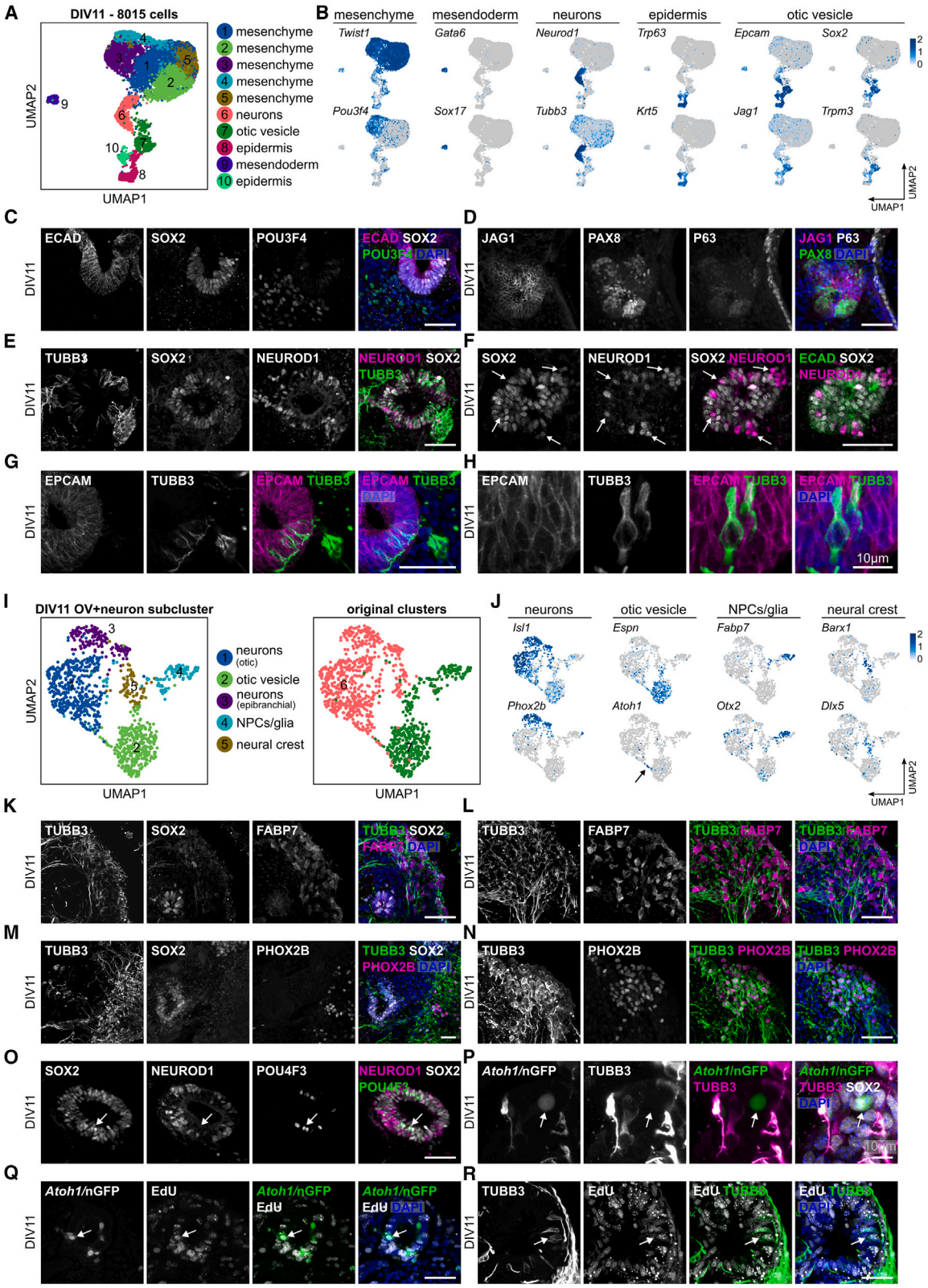

(legend on next page)

development.[17,22,23] To further isolate this population of cells, we subclustered DIV11 otic vesicle cells and neurons (DIV11 clusters 6 and 7, Figure 3A). This analysis revealed a small population of *Sox2*+/*Otx2*+/*Fabp7*+ NPCs/glia (cluster 4, Figures 3I–3L) that originally co-clustered with *Sox2*+ otic vesicle cells, as well as a cluster of presumed neural crest cells (cluster 5) that expressed neural crest transcription factors *Barx1* and *Dlx5* (Figure 3J).[24,25] The TUBB3+ neuronal cells were separated into two clusters (clusters 1 and 3), both of which were determined to be placodal-derived neurons based on *Isl1* expression (Figure 3J). However, the smaller cluster of *Isl1*+ neurons also expressed the geniculate ganglion marker *Phox2b* (Figures 3J, 3M, and 3N), suggesting that cluster 3 neurons are likely epibranchial-derived, whereas cluster 1 neurons are otic-derived.[17]

Espn+ otic vesicle cells (cluster 2) cleanly separated from the *Isl1*+/*Phox2b*-otic-derived neuron cluster, albeit with a small branch made up of cells from a mix of originally annotated otic vesicle and neuron cells (Figure 3J).[20] Closer inspection of these cells unexpectedly revealed the expression of hair cell genes such as *Atoh1* (Figure 3J, arrow). This observation spurred our interest in assessing if organoid otic vesicle structures are already producing hair cells in addition to neuroblasts at DIV11. Co-staining for the hair cell transcription factor POU4F3 and neuronal transcription factor NEUROD1 in DIV11 organoids indeed revealed POU4F3+/NEUROD1- hair cells within SOX2+ otic vesicle structures (Figure 3O). This is consistent with the roles of POU4F3 and its downstream target GFI1 in repressing neuronal gene expression.[26,27] We next utilized the *Atoh1*/nGFP mESC line to generate inner ear organoids in which developing hair cells express nuclear GFP under the control of an *Atoh1* enhancer.[28] Staining of *Atoh1*/nGFP organoids at DIV11 further revealed that nGFP-expressing cells do not express TUBB3, suggesting that TUBB3+ cells within otic vesicle-like structures are delaminating neuroblasts rather than nascent hair cells (Figure 3P). Finally, to assess whether DIV11 hair cells and neuroblasts were simultaneously being generated by the proliferation of otic vesicle progenitor cells, we applied 10μM EdU for 2 h at DIV10 and collected organoids at DIV11. This revealed both EdU+/*Atoh1*/nGFP+ hair cells and EdU+/TUBB3+ neuroblasts (Figures 3Q and 3R), confirming that both cell types differentiated from otic progenitors that were actively proliferating within otic vesicle structures at DIV10.

Cell populations stabilize in DIV16 and DIV21 mESC-derived inner ear organoids

After DIV11, otic vesicle structures mature into simple sensory epithelia, complete with vestibular-like MYO7A+ hair cells and underlying SOX2+/JAG1+ supporting cells by DIV14 (Figure 1D).[3] Assessing the full composition of organoid cell types at DIV16 revealed a large, maintained population of *Twist1*+ mesenchymal cells (DIV16 clusters 1, 2, 4, and 9, 54.5%), some of which also expressed the otic mesenchyme marker POU3F4+ as seen at DIV11 (Figures 4A–4C, Data S1). Additionally, the mesendoderm population present from DIV3 to DIV11 likely transitioned into *Myod1*+/*Myog*+ muscle cells by DIV16 (DIV16 clusters 5 and 13, 9.0%, Figure 4B).[29] Similar to what was seen at DIV11, there is also evidence of co-clustered populations of *Tubb3*+ neurons and *Fabp7*+ glia (DIV16 cluster 10, 3.7%), as well as a large population of *Trp63*+ epidermal cells (DIV16 clusters 3, 6, 7, 11, and 12, 27.8%), which now also included more advanced epidermal subtypes such as *Krt14*+ keratinocytes (Figure 4D). Finally, we identified two groups of *Sox2*+/*Fbxo2*+ otic cells: supporting cells (DIV16 cluster 8, 4.2%) and *Myo7a*+/*Atoh1*+ hair cells (DIV16 cluster 14, 0.7%) (Figures 4A and 4B).[30] The hair cells in DIV16 organoids are SOX2+, POU4F3+, and CALB2+ (Figures 4E–4G); however, F-actin labeling using phalloidin revealed the variable presence of hair bundles, suggesting these hair cells are immature (Figure 4H).

No significant changes to cell composition were seen between DIV16 and DIV21 in our scRNA-seq. The majority of cells in DIV21 organoids are *Twist1*+ mesenchymal cells (DIV21 clusters 1, 2, 4, 5, and 9, 61.9%) (Figures 4I and 4J, Data S1). DIV21 organoids also contain populations of *Myod1*+/*Myog*+ muscle cells (DIV21 clusters 3, 6, and 11, 20.0%) and *Trp63*+ epidermal cells (DIV21 clusters 7 and 8, 11.6%). Neurons and glia make up a small proportion of total cells (DIV21 cluster 12, 1.7%); however, low capture of these cells in our later-stage scRNA-seq data is likely a reflection of the sensitivity of these cells to dissociation rather than reduced prevalence in the organoids themselves. Finally, we also identified populations of *Sox2*+/*Fbxo2*+ supporting cells (DIV21 cluster 10, 4.2%) and *Myo7a*+/*Atoh1*+ hair cells (DIV21 cluster 13, 0.5%). EPCAM+ sensory epithelial structures in DIV21 organoids are flanked by EPCAM+/P63+ epidermal cells and contain SOX2+ supporting cells and MYO7A+/PVALB+/CALB2+/OTOF+ hair cells (Figures 4K–4N). A summary

Figure 3. scRNA-seq of DIV11 organoids followed by subclustering of neurons and otic vesicle-like cells reveals simultaneous hair cell and otic neuroblast formation

(A and B) scRNA-seq of DIV11 organoids shows the formation of *Epcam*+/*Sox2*+/*Jag1*+/*Trpm3*+ otic vesicle cells, in addition to mesendoderm, mesenchyme, neurons, and epidermis.

(C and D) Validation of POU3F4+ mesenchymal cells and P63+ epidermis developing adjacent to SOX2+/PAX8+/JAG1+ otic cells at DIV11.

(E–H) Staining for the neuronal markers TUBB3 and NEUROD1 revealed delaminating neuroblasts within otic vesicle-like structures. White arrows denote SOX2+/NEUROD1+ otic vesicle cells.

(I and J) Subclustering of DIV11 otic vesicle and neuronal cells revealed distinct populations of *Isl1*+/*Phox2b*+ epibranchial and *Isl1*+/*Phox2b*- otic neurons, as well as neural precursor cells (NPCs)/glia, and neural crest cells that originally clustered with otic vesicle cells. Black arrow denotes a small population of *Atoh1*+ otic vesicle cells.

(K–N) Validation of FABP7+ glia and PHOX2B+ epibranchial neurons in DIV11 organoids.

(O) Validation of POU4F3+/NEUROD1- hair cells (white arrows) in DIV11 otic vesicle-like structures.

(P) Nascent hair cells express *Atoh1*/nGFP and are TUBB3- (white arrows).

(Q and R) Treatment of organoids with a 2-h pulse of EdU at DIV10 reveals that both *Atoh1*/nGFP+ hair cells and TUBB3+ neuroblasts are generated from actively proliferating otic lineage cells, as shown by the presence of nuclear EdU at DIV11 (white arrows). Scale = 50 μm unless otherwise stated, $n \geq 3$.

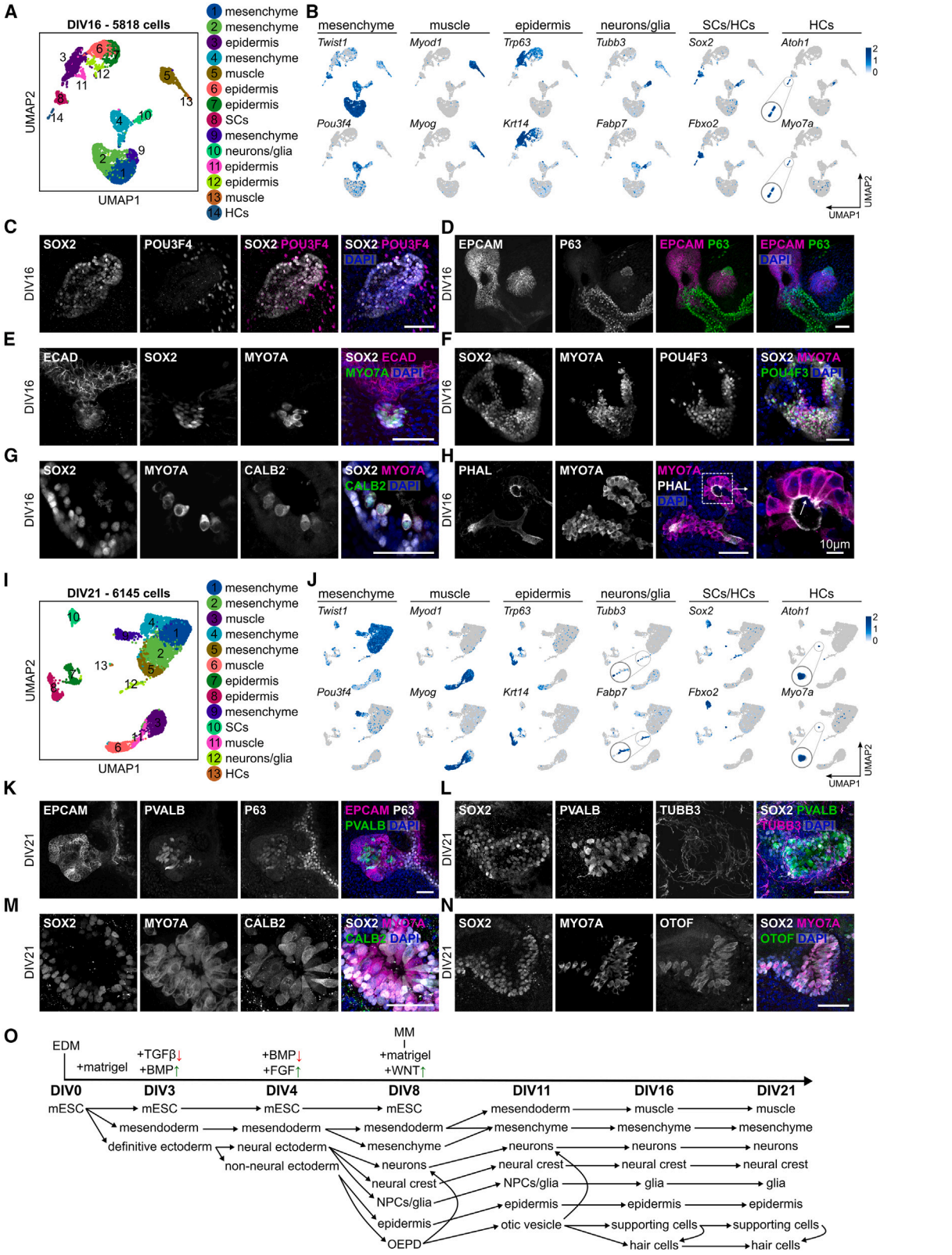

(legend on next page)

of the identified cell groups from DIV3 to DIV21 organoid development is provided in Figure 4O.

Combined analysis of otic lineage cells reveals minimal hair cell differences between DIV16 and DIV21

To assess gene expression in developing organoid hair cells, we next combined all otic-lineage cells from our DIV11 (Figure 3I cluster 2), DIV16 (Figure 4A clusters 8 and 14), and DIV21 (Figure 4I clusters 10 and 13) time points using Seurat's *Integration* feature.[31] This revealed a small population of *Dlx5*+/*Barx1*+ presumed neural crest cells that originally co-clustered with otic lineage cells mainly at DIV16 and DIV21, which were removed from subsequent analysis. We next re-clustered the remaining cells and visualized them using similarity weighted nonnegative embedding (SWNE), a method for visualizing high-dimensional data that can aid in biological interpretation.[32] Combining otic lineage cells from each time point resulted in a surprising overlap of *Sox2*+ DIV11 otic vesicle cells with *Sox2*+ DIV16 and DIV21 supporting cells across 4 clusters, as well as one cluster of *Myo7a*+ hair cells (Figures 5A and 5B). All clusters had representation from each time point (Figure 5C). We first assessed the differences in gene expression between hair cells and their underlying otic vesicle/supporting cells at each time point. This analysis firstly showed that DIV11 hair cells upregulate a neurosensory competent transcriptional program that includes both hair cell and neuronal transcription factor genes such as *Neurog1*, *Neurod1*, *Insm1*, *Atoh1*, and *Pou4f3* (Figure 5D, Data S1)[17,26,27,33–36]. At the later DIV16 and DIV21 time points, underlying supporting cells took on more distinct gene expression profiles, with increased expression of *Otoa* and *Otol1* compared to *Atoh1*+/*Pou4f3*+/*Gfi1*+ hair cells.[37,38] Furthermore, a comparison DIV11 otic vesicle cells to combined DIV16 and DIV21 supporting cells showed the downregulation of otic vesicle/early supporting cell genes such as *Sox11* and cell cycle genes such as *Top2a* and *Ccnd2* as sensory epithelial structures developed (Figure 5E).[39,40] This progressive development of supporting cells is also seen between DIV16 and DIV21, with further repression of *Sox11* and *Top2a* and upregulation of supporting cell genes *Otoa*, *Otol1*, and *Tecta* (Figure 5E).[37,38]

A comparison of DIV11 hair cells to combined DIV16 and DIV21 hair cells revealed the downregulation of neuronal genes such as *Neurog1*, *Neurod1*, and *Insm1* as organoid hair cell development progressed (Figures 5F and S2, and Data S1).[17] This was concurrent with the further upregulation of canonical hair cell genes, such as *Atoh1*, *Pou4f3*, and *Gfi1*.[26] Considering that DIV11 otic vesicles produced neuroblasts at this stage (Figures 3E–3H), it is possible that 1) early differentiating hair cells exhibit a shared neuronal gene expression profile with early neuroblasts, or 2) some early-stage neuroblasts from DIV11 co-cluster with early-stage hair cells. Finally, and most surprisingly, a comparison of DIV16 hair cells to DIV21 hair cells revealed little differences in gene expression (Figure 5F), suggesting that either DIV16 hair cells represent fully mature organoid hair cells or, more likely, that organoid hair cell maturation is stalled after DIV16.

The proliferative potential of otic cells within inner ear organoids decreases over time

We next aimed to assess the dynamic changes in gene expression that occur as otic vesicle cells from DIV11 develop into supporting cells and hair cells at DIV16 and DIV21. For this, we utilized the trajectory analysis tool Slingshot[41] to predict the developmental lineages stemming from cluster 4 of the combined otic dataset (Figure 5A), as it contained the highest percentage of DIV11-derived cells (74%, Figure 5C). This analysis revealed two developmental lineages (Figures 5G and 5H). Lineage 1 terminates at cluster 3, which contains the highest proportion of DIV21 supporting cells of all the combined clusters (51%, Figure 5C), and lineage 2 terminates at cluster 5, which contains hair cells.

We next utilized tradeSeq[42] to assess which genes are differentially regulated along pseudotime for each lineage (tradeSeq's Association Test). These genes were then grouped according to their patterns of gene expression. Lineage 1 group 1 contains 132 genes that are initially highly expressed at the start of pseudotime (containing mainly DIV11 otic vesicle cells) and then downregulated (Figure 5I, Data S2). Gene ontology (GO) analysis showed that these genes are significantly associated with cell division, which is in concordance with our EdU experiments that showed DIV11 organoids are highly proliferative (Figures 3Q and 3R, Data S3). The next three groups of genes differentially regulated along lineage 1 (group 2 = 43 genes, group 3 = 53 genes, and group 4 = 147 genes) are initially lowly expressed, are upregulated, and subsequently downregulated. These genes are associated with supporting cell developmental GO terms such as pattern specification, tube morphogenesis, and actin filament organization, and include prosensory and supporting cell genes such as *Jag1*, *Sox11*, and *Tmsb4x*.[20,37,40,43] Finally, the last two groups are upregulated toward the end of lineage 1 pseudotime (group 5 = 425 genes, group 6 = 96 genes) and, like groups 2–4, contain genes associated with GO terms such as actin filament-based process and pattern specification, as

Figure 4. scRNA-seq of DIV16 and DIV21 inner ear organoids

(A and B) scRNA-seq of DIV16 organoids shows the formation of *Epcam*+/*Sox2*+/*Fbxo2*+ supporting cells (SCs) and *Epcam*+/*Sox2*+/*Fbxo2*+/*Myo7a*+ hair cells (HCs), in addition to muscle, mesenchyme, neurons/glia, and epidermis.

(C and D) Validation of POU3F4+ mesenchymal cells and P63+ epidermis adjacent to sensory epithelia at DIV16.

(E–H) Organoid sensory epithelia consist of ECAD+/SOX2+ supporting cells surrounding ECAD+/SOX2+/MYO7A+/POU4F3+/CALB2+ hair cells. Hair cells at DIV16 rarely displayed phalloidin (PHAL)+ hair bundles.

(I and J) scRNA-seq of DIV21 organoids showed stable cell populations compared to DIV16.

(K–N) DIV21 sensory epithelia consist of EPCAM+/SOX2+ supporting cells surrounding EPCAM+/MYO7A+/PVALB+/OTOF+ hair cells, with variable expression of CALB2 and SOX2. Sensory epithelia are surrounded by TUBB3+ neurites. Scale = 50 μm unless otherwise stated, $n \geq 3$.

(O) Summary of the DIV3-DIV21 inner ear organoid scRNA-seq atlas. EDM, ectodermal differentiation media; mESCs, mouse embryonic stem cells; MM, maturation media; ↓, inhibition; ↑, activation; NPCs, neural precursor cells; OEPD, otic-epibranchial progenitor domain.

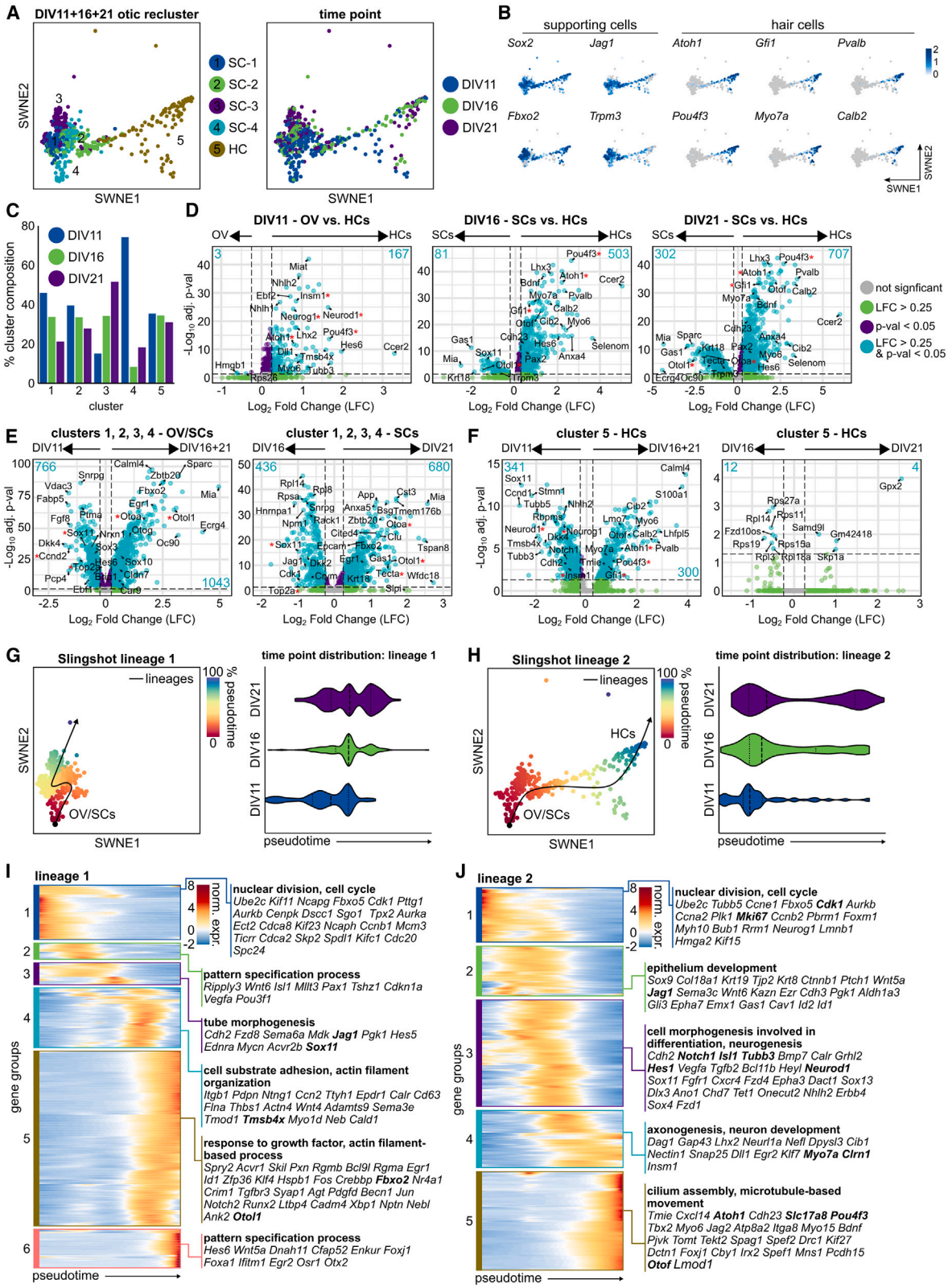

(legend on next page)

well as response to growth factor. These groups also contain known supporting cell genes such as *Fbxo2* and *Otol1*.[20,30]

Similar to lineage 1 group 1, lineage 2 group 1 contains 236 genes significantly associated with cell cycle progression that are initially highly expressed at the start of pseudotime (Figure 5J, Data S2 and S3), including well-characterized cell cycle genes such as *Cdk1* and *Mki67*.[39] The next two differentially regulated gene groups of lineage 2 (group 2 = 213 genes, group 3 = 453 genes) demonstrate a peak of expression in the middle of the trajectory and are associated with GO terms such as epithelium development, cell morphogenesis involved in differentiation, and neurogenesis. These groups include genes such as the inner ear prosensory genes *Jag1* and *Isl1*, other Notch signaling components such as *Notch1* and *Hes1*, as well as neuronal genes such as *Neurod1* and *Tubb3* (Figure 5J).[17,44,45] Lineage 2 groups 4 (244 genes) and 5 (422 genes) consist of genes that are turned on toward the end of the trajectory as supporting/prosensory cells transition to hair cells. These genes are significantly associated with GO terms such as neuron development and cilium assembly, and include many known hair cell genes such as *Clrn1*, *Myo7a*, *Atoh1*, *Pou4f3*, *Slc17a8*, and *Otof* (Figure 5J).[22,46–49]

After observing a rapid downregulation of cell cycle gene expression at the onset of both the supporting cell and hair cell developmental lineages (Figure 5I gene group 1; Figure 5J gene group 1), we hypothesized that the proliferative potential of inner ear organoid cells decreases as the organoid ages. To assess this hypothesis, we first used *Seurat* to annotate the cell cycle phase of each cell in our combined DIV11, DIV16, and DIV21 otic dataset. Stratifying by time point, we observed that DIV11 otic vesicle cells contained the greatest proportion of cells in the G2/M and S phases of the cell cycle, whereas the majority of cells at DIV21 are in G1 (Figure 6A). We next stained organoids from each time point with antibodies to the proliferation marker Ki67 (Figure 6B).[39] Quantification of Ki67+ otic epithelium cells at DIV11 and DIV16 revealed no statistical differences, with approximately 80–85% of cells expressing nuclear Ki67 (Figure 6C). However, by DIV21, Ki67+ otic cells were significantly decreased, with less than 2% of otic cells exhibiting positive nuclei (Figures 6C and 6G).

We next investigated the potential cause of Ki67 downregulation in DIV21 organoids. In the inner ear, the cell cycle inhibitor $p27^{Kip1}$ maintains the proliferative quiescence of both cochlear and vestibular supporting cells.[50] Within our scRNA-seq data, the gene encoding $p27^{Kip1}$ (*Cdkn1b*) is more highly expressed in DIV21 otic cells compared to DIV11 and DIV16 (Figure 6D). Staining and quantification of $p27^{Kip1}$ in organoids further confirmed this expression data and complements the observed decrease in Ki67 expression at DIV21; DIV11 and DIV16 otic cells expressed similar levels of $p27^{Kip1}$ (5–20% $p27^{Kip1}$+ nuclei), but by DIV21, the number of positive nuclei greatly increased (approximately 60% $p27^{Kip1}$+ nuclei) (Figures 6E and 6F). We did not observe expression of $p27^{Kip1}$ in all otic cell nuclei, as most hair cells do not express high levels of nuclear $p27^{Kip1}$ compared to supporting cells (Figure 6H). These observations confirm that the proliferative potential of otic lineage cells decreases over time, with almost a complete loss of inner ear organoid growth potential by DIV21. We hypothesize that upregulation of *Cdkn1b*/$p27^{Kip1}$ in DIV21 otic lineage cells restricts the continuing growth of the sensory patches.

Comparison to utricle-derived hair cells reveals arrested maturation of organoid-derived hair cells

Our Slingshot trajectory analysis suggests that organoid hair cells undergo a generic hair cell developmental program, which includes the upregulation of hair cell transcription factors such as *Atoh1* and *Pou4f3*, followed by the expression of functional hair cell genes like *Myo7a*, *Cdh23*, and *Pcdh15* (Figure 5J).[22,47,51] Additionally, our differential gene expression analyses suggest that surprisingly few molecular changes occur within hair cells between DIV16 and DIV21 (Figure 5F). We therefore next aimed to assess the extent of organoid hair cell maturation at DIV21 by comparing them to *in vivo* derived hair cells. For this analysis, we combined our organoid hair cell single-cell profiles (Figure 5A, cluster 5) with utricle hair cell profiles from postnatal days (P) 1, P12, and P100 mice (see STAR Methods).[52] This integration showed an overlap of DIV21 organoid hair cells with immature P1 mouse utricle hair cells (Figures 7A and 7B). However, despite this overlap, differential gene expression analysis revealed significant differences between DIV21 organoid hair cells compared to immature, type I and type II utricle-derived hair cells (Figures 7C–7E, Data S1). A repeat of this analysis using a separate dataset of utricle hair cells from P2, P4, and P6 mice

Figure 5. Pseudotime trajectory analysis of DIV11, DIV16, and DIV21 otic cells reveals supporting cell and hair cell developmental trajectories

(A and B) Combination and reclustering of DIV11, DIV16, and DIV21 otic lineage cells results in four clusters of *Sox2*+/*Jag1*+ otic vesicle/supporting cells and one cluster of *Atoh1*+/*Pou4f3*+/*Gfi1*/*Myo7a*+ hair cells.

(C) Each cluster is made up of cells from each time point.

(D) Comparison of hair cells to underlying otic vesicle/supporting cells at each time point reveals minimal differences between DIV11 otic vesicle vs. DIV11 hair cells, albeit for upregulation of neuronal and hair cell genes (see Data S1). At DIV16 and DIV21, hair cells and supporting cells show more distinct gene expression patterns. Blue values denote the total number of genes reaching the significance threshold, and red asterisks denote specific genes mentioned in the text.

(E and F) Both otic vesicle/supporting cells and hair cells undergo developmental changes in gene expression, except for hair cells between DIV16 and DIV21, which show minimal differences. OV, otic vesicle; SC, supporting cell; HC, hair cell.

See also Figure S2.

(G) Slingshot trajectory analysis predicts a developmental lineage (lineage 1) starting within the combined dataset cluster 3 (high % DIV11) and ending in cluster 2 (high % DIV21), representing potential supporting cell maturation.

(H) Slingshot also predicts a second developmental lineage (lineage 2) starting within the combined dataset cluster 3 (high % DIV11) and ending in cluster 4 (hair cells), representing potential otic vesicle to supporting cell to hair cell development.

(I and J) Differentially regulated gene expression analysis reveals 896 genes differentially regulated along lineage 1, and 1,568 genes differentially regulated along lineage 2 (see Data S2). These genes are separated into 6 and 5 groups, respectively, based on similar gene expression patterns along pseudotime. Significantly enriched gene ontology terms for each gene group are shown in bold, with example genes in italics (see Data S3). Genes in bold are specifically mentioned in the text.

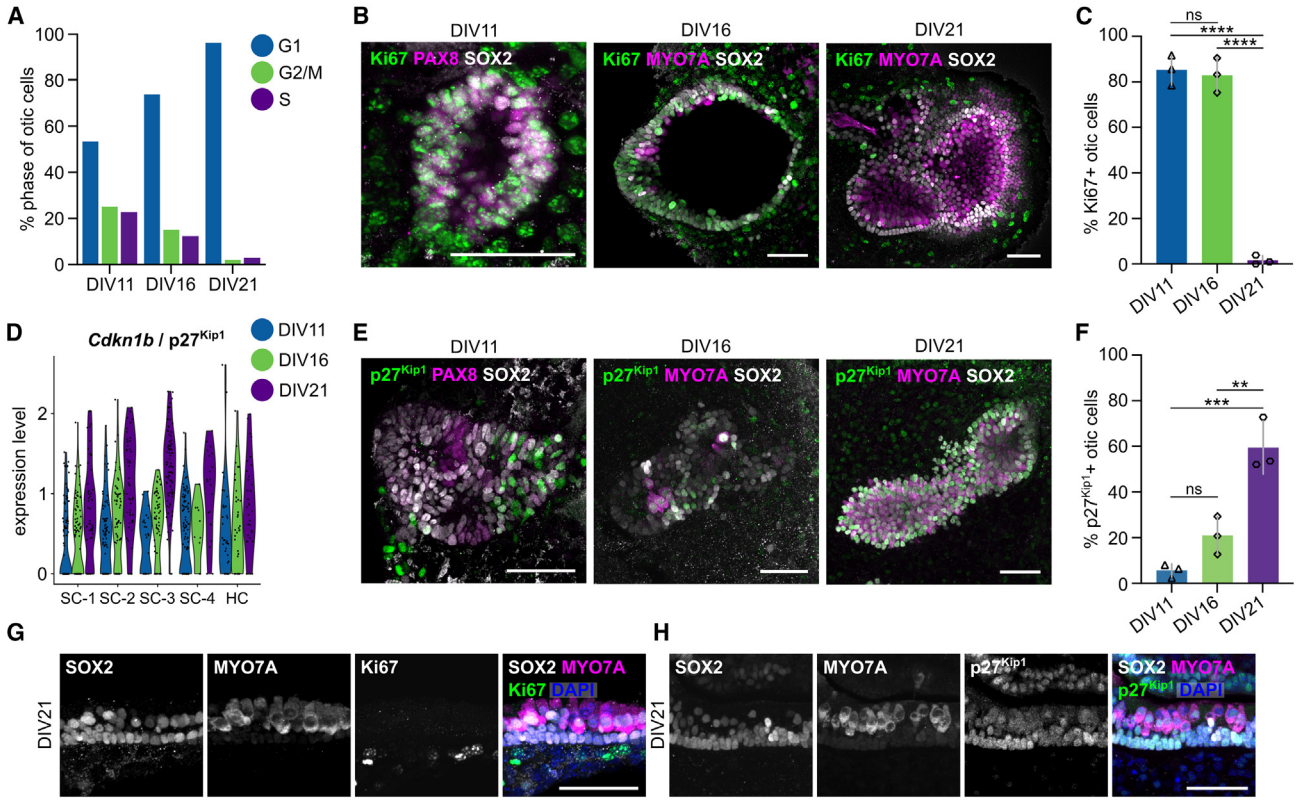

Figure 6. The proliferative potential of organoid otic lineage cells decreases with time, likely due to increased p27^{Kip1} expression

(A) Cell cycle phase annotation of otic lineage cells at DIV11, DIV16, and DIV21.

(B and C) The percent of Ki67+ cycling otic lineage cells decreases between DIV16 and DIV21. Boundaries of the quantified otic vesicle/sensory epithelia regions were determined by SOX2 expression. Scale = 50 μm, $n = 3$. p value ****<0.0001, ns = not significant. Significance was assessed by ordinary one-way ANOVA followed by Tukey's multiple comparisons test. Data are represented as mean ± SD.

(D) *Cdkn1b*, which encodes for the cell cycle inhibitor p27^{Kip1}, is more highly expressed in DIV21 otic lineage cells.

(E and F) p27^{Kip1} expression significantly increases in otic lineage cells between DIV16 and DIV21. Scale = 50 μm, $n = 3$. p-value **<0.01, ***<0.001, ns = not significant. Significance was assessed by ordinary one-way ANOVA followed by Tukey's multiple comparisons test. Data are represented as mean ± SD.

(G and H) Magnified cross-sections of DIV21 vestibular-like sensory epithelia showing no SOX2+/Ki67+ cells and many SOX2+/p27^{Kip1}+ cells. MYO7A + hair cells show variable nuclear expression of p27^{Kip1}. Scale = 50 μm, $n = 3$.

(Figure S3)[37] produced similar results; DIV21 hair cells overlapped with hair cell precursors and type II hair cells, but still exhibited many differentially regulated genes when compared with utricle hair cell subtypes directly (Figure S3, Data S1). This suggests that organoid hair cells, in this experimental context, do not exhibit distinguishing molecular phenotypes of mature utricle hair cell subtypes.

DISCUSSION

Inner ear organoids can be reliably generated from mESCs, with mechanosensitive hair cells resembling vestibular-like hair cells of the postnatal mouse detectable within three weeks.[53] Using a previously validated guidance protocol,[3] we observed that experiment-to-experiment variability in the time course and extent of inner ear tissue differentiation was low; for example, we consistently observed POU4F3+ hair cell and TUBB3+ neuroblast formation within SOX2+ otic vesicle-like structures at DIV11 (Figures 3O–3R), and MYO7A + hair cells within SOX2+ sensory epithelia-like structures at DIV16 and 21 (Figures 4E–4G, 4M, and 4N). We reason that this robustness is an advantage of using mouse cells over human cells, as human inner ear organoid differentiation can be more variable due to protracted culture periods of 30–100 days.[54] Additionally, conclusions made from the study of mESC-derived vestibular-like inner ear organoids likely have direct applicability to human inner ear organoids due to similarities in the differentiation protocols and generated cell types.[38,54]

Here, we performed scRNA-seq at distinct time points of vestibular-like inner ear organoid formation. These time points were selected based on the proposed progression of pre-placodal and placodal otic progenitor development in three-dimensional culture.[3,8] Through our analysis of over 30,000 cells from six distinct time points, we were able to identify transcriptional profiles of previously postulated developmenting tissues that recapitulate *in vivo* inner ear development, including non-neural ectoderm and otic-epibranchial progenitor domain cells, followed by proliferating otic prosensory progenitors and ultimately

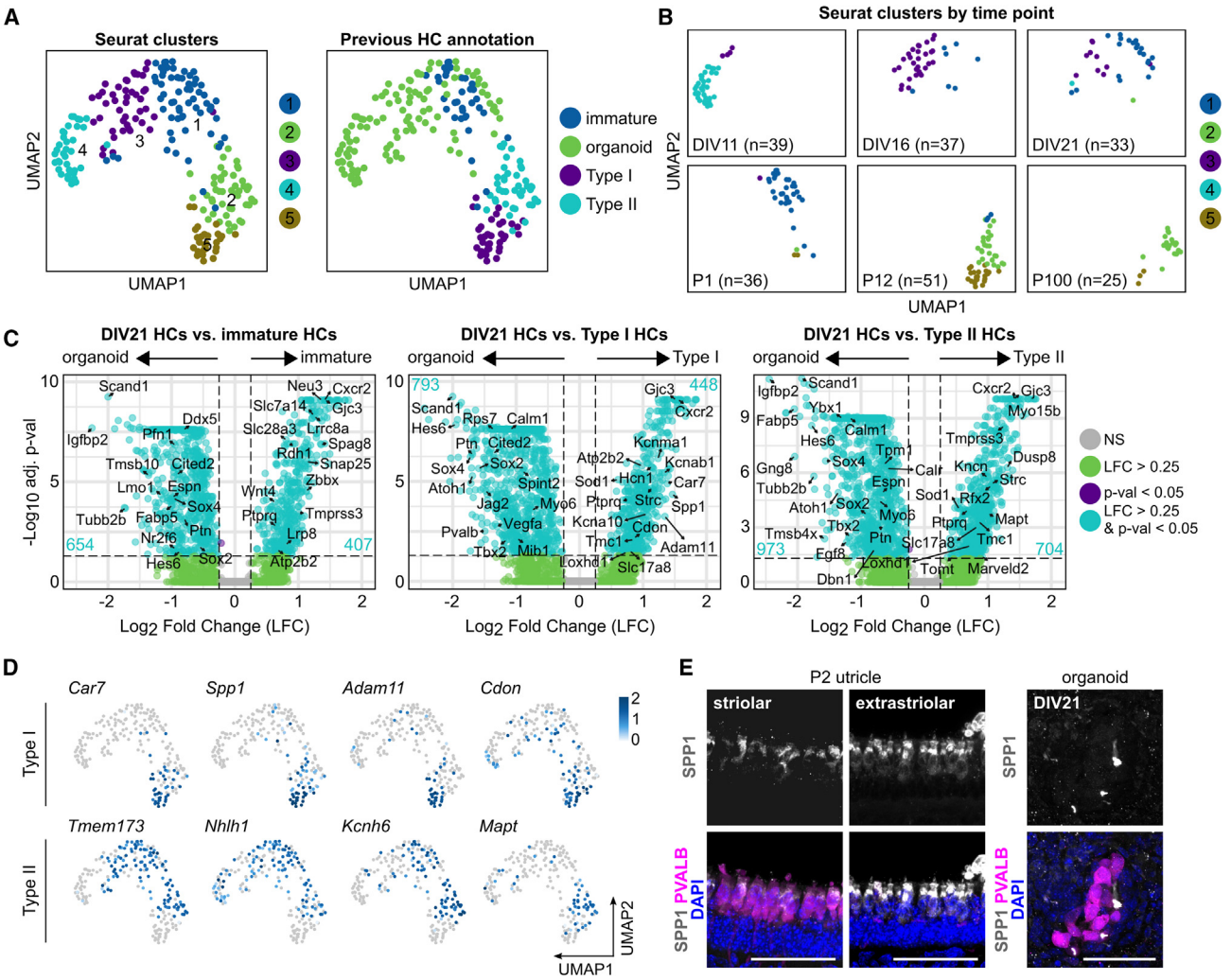

Figure 7. Comparison of organoid hair cells to *in vivo* derived hair cells reveals substantial molecular differences

(A and B) Single-cell profiles of organoid hair cells (HCs) from DIV11, DIV16, and DIV21 organoids (Figure 5A, cluster 5) were combined with utricle hair cell profiles from postnatal day (P) 1, P12, and P100 mice. Clustering revealed an overlap of DIV21 hair cells (the most mature organoid time point) mainly with annotated immature hair cells from P1 utricles.

(C) Differential gene expression analysis of DIV21 hair cells compared to *in vivo*-derived immature, type I and type II utricle hair cells. Blue values denote the total number of genes reaching the threshold of significance.

(D and E) Example marker genes for mature type I and type II hair cells. While many type II hair cell markers are also expressed within immature and organoid hair cells, mature type I and type II markers, such as *Spp1* and *Mapt*, are not expressed in organoid hair cells.

See also Figure S3. Scale = 50 μm, $n \geq 3$.

differentiating vestibular-like sensory epithelia. These cell groups are complemented by non-otic tissues that likely provide scaffolding and a supportive environment for the robust differentiation of inner ear cell types. Our scRNA-seq datasets and the temporal map of otic differentiation in the organoid serve as valuable resources for future studies and can help identify specific stages where modifications to the protocol can be made to increase efficiency.

Similar to the recent report on developmental trajectories of otic lineage cells from hESC-derived organoids[18,55] and the recent comparison of hESC-derived inner ear organoids to the developing fetal inner ear,[38,56] our analyses suggest that mESC-derived inner ear organoids are generally suitable for comparison with *in vivo* mouse otic lineage development, tissue growth, and differentiation of the major inner sensory epithelia cell types (i.e., generic hair cells and supporting cells). This observation is significant, as it increases confidence in translating discoveries made in the inner ear organoid model into the *in vivo* context. Moreover, because organoids are easily accessible and manipulatable, we argue that—especially for inner ear biology where tissue is scarce—they provide a valuable model system. Our datasets, as well as our findings, provide a useful context for such future studies.

Lineage development

With respect to lineage development, we found that the initial guidance cues of the protocol resulted in the generation of >70% of ectodermal lineage cells and a small (<1%) group of mesendoderm cells at DIV3. Expression of neural ectoderm markers such as *Pou3f1* (Figure 2A, Zhu et al., 2014) suggests that, without intervention, neural ectoderm is likely the primary cell fate within the early stages of this protocol. However, the addition of BMP and TGFβ inhibition at DIV3 results in the rapid induction of the non-neural ectoderm lineage, as denoted by *Gata3* and *Tfap2a* expression by DIV4 (Figure 2D).[14] Using qPCR, we further showed that the non-neural ectoderm population also quickly transitioned into *Pax8*+ pre-placodal ectoderm as well as *Trp63*+ surface ectoderm after the addition of FGF and a BMP inhibitor at DIV4 (Figure 2M). Our analysis suggests that it is potentially possible to affect the branching of pre-placodal ectoderm and surface ectodermal lineages between DIV4 and DIV8. This could be done by screening compounds that affect the lineage switch toward pre-placodal ectoderm and away from surface ectoderm by adding them to the culture media at DIV4. On the other hand, it remains to be determined whether suppression of surface ectoderm would be beneficial for expanding the pre-placodal population. Non-otic ectodermal lineages might be essential for stabilizing and maintaining otic lineages, perhaps through paracrine signaling within the organoid. By DIV8, we identified distinct otic placodal (otic-epibranchial progenitor domain) and surface ectoderm lineages at approximately equal ratios, accounting for about one-quarter of the whole organoid (Figures 2G and 2H).

Tissue growth

Whereas the initial week of organoid formation, up to DIV8, is dominated by the progression of the ectodermal lineage toward otic-epibranchial progenitor domain cells and organoid growth, by DIV11 we began observing cell cycle exit of some sensory progenitors that differentiated into early hair cells. This suggests that switching culture conditions at DIV8 from ectodermal induction media to maturation media results in an environmental change that leads to the production of postmitotic sensory epithelial cells in addition to the continuing proliferation of otic progenitors. This process is likely also affected by natural growth limitations with respect to organoid size, as well as by the removal of growth factors. It is notable that the formation of otic vesicle-like cells at DIV11 revealed several processes that appeared to be happening in parallel as the organoids further developed. Our temporal trajectory analysis showed that the pro-sensory cell population at DIV11 was robustly proliferating (Figures 5I and 5J), which we interpret as a phase of continued expansion of otic tissue. In parallel, however, we identified distinct populations of hair cells and neuroblasts that arose from proliferating progenitors (Figures 3E–3H, 3O, and 3P), which were labeled when EdU was provided in a 2 h pulse at DIV10 (Figures 3Q and 3R). With the progressing maturation of organoids at DIV16 and, ultimately, at DIV21, the gene expression within the otic population changed substantially (Figures 5E, 5I and 5J). Markers of proliferation were replaced by genes associated with cell differentiation and epithelial/neural tissue specification expected to be found in emerging sensory epithelia (Figures 5I and 5J). This observation was further validated by the downregulation of the proliferation marker Ki67 between DIV16 and DIV21 (Figures 6B and 6C).

Based on these observations, we conclude that the early otic vesicle-like epithelial cell groups in DIV10-11 organoids represent an interesting transient stage. Interesting, in the sense that they express a variety of otic markers lacking hair cell or neuronal genes and resemble, to some extent, supporting cells. These cells proliferate and contribute to the expansion of the otic domains within the organoid that ultimately harbor hair cells and supporting cells at DIV16-21. Likewise, they generate a considerable population of neurons that display gene expression profiles consistent with otic neurons (i.e., *Isl1*+/*Phox2b*-, Figures 3I and 3J). Gene expression analysis within these cell groups suggests that known signaling pathways, most notably Notch, are active during these processes of balancing progenitor cell proliferation and cell differentiation (Figure 5J). Further investigation of the proliferating otic epithelial cell population at DIV10-11, and finding culture conditions that might stabilize their growth and suppress the early differentiation of hair cells and neuroblasts, could provide a biotechnological opportunity to enrich for proliferating ESC-derived otic tissue.

Differentiation

The hallmark of inner ear sensory epithelia is their composition of two distinct cell types: hair cells and supporting cells. This duo is complemented by afferent otic neurons that delaminate from a common neurosensory progenitor population within the anterior-ventral otic vesicle during inner ear development.[17] Our analyses suggest that this trio of cell types is also generated in inner ear organoids, with hair cells and neuroblasts forming within SOX2+ otic vesicle-like structures already at DIV11 (Figure 3). Our developmental trajectory analysis of DIV11 otic vesicle cells and DIV16 and DIV21 supporting cells and hair cells suggests that, within the organoids, cycling otic progenitors progress through an intermediate prosensory cell fate before ultimately differentiating into hair cells. This is evidenced by a downregulation of cell cycle genes, followed by a temporary upregulation of prosensory/supporting cell genes such as *Jag1* and *Hes1*, and subsequently an upregulation of hair cell transcription factors such as *Atoh1* and *Pou4f3* (Figure 5J). However, it is unclear if organoid supporting cells at later stages are capable of directly transdifferentiating into hair cells. Based on the downregulation of proliferative markers and upregulation of cell cycle inhibitors such as p27Kip1 in DIV21 organoids (Figure 6), transdifferentiation would likely be the primary mode of hair cell generation in later-stage organoids. Future work utilizing lineage tracing of supporting cells will be necessary to assess if organoids beyond DIV21 can add new hair cells. Additionally, studies to determine if late-stage organoid supporting cells are capable of re-entering the cell cycle to robustly produce new hair cells would also be of interest, as there is no such mechanism in the *in vivo* mammalian inner ear.

In conclusion, here we present a single-cell RNA-seq atlas of developing mESC-derived inner ear organoids spanning ectoderm formation to hair cell development. These data represent a useful resource for inner ear biologists seeking to utilize this model for studying and manipulating inner ear

cell type-specific development. Furthermore, our work complements a growing number of datasets demonstrating the utility of both human and mouse inner ear organoid models for such studies.[5,7,18,38,55–58] For example, mESC-derived inner ear organoids can be used to test mechanisms for inducing mammalian supporting cell proliferation after DIV21, when the majority of supporting cells are post-mitotic (Ki67− and p27Kip1+). The profiling of whole organoids at each time point, compared to solely assessing sorted otic lineage cells, also opens the door for studying the effect of co-developing cell types, such as epidermis and otic mesenchyme, on otic lineage cells at different time points. Assessing the source of potential inhibitory internal signaling could identify additional small molecules to be incorporated into existing protocols to increase the efficiency of otic lineage development or to induce cochlear versus vestibular fate.

Limitations of the study

Our developmental atlas was generated by profiling all cells within mESC-derived inner ear organoids at all time points. While this strategy provides useful context for otic lineage development within the organoids as a whole system, it limited our resolution to profile many organoid hair cells for our *in vivo* comparisons. It is perhaps for this reason that we were unable to identify the differentiation of more mature vestibular hair cell subtypes, such as type Is and type IIs, which have previously been reported in both mESC- and hESC-derived inner ear organoids.[53,56] Indeed, a recent complementary study of sorted cells from DIV16, DIV20, and DIV21 *Atoh1*/nGFP mESC-derived vestibular-like organoids, which profiled over 3,000 hair cells, was able to identify transcriptional profiles associated with vestibular type I and type II hair cell identities, as well as cochlear outer hair cells.[57] In addition to a lack of resolution in this study, factors such as additional culture time and different starting cell lines may also affect the formation of more mature hair cells in the inner ear organoid model.

RESOURCE AVAILABILITY

Lead contact

Further information and requests for reagents may be directed to the lead contact, Maggie S. Matern (mmatern@stanford.edu).

Materials availability

The study did not generate new unique reagents.

Data and code availability

- Single-cell RNA-seq data are stored in ten Seurat objects provided as Data S1 through S10. These data have been deposited to Mendeley Data: https://doi.org/10.17632/tgsssyzwwg.1.
- The data have also been deposited to the Gene Expression Omnibus (GEO: GSE252570) as well as the Gene Expression Analysis Resource portal (umgear.org).[59]
- No original code was developed.
- Any additional information required to reanalyze the data reported in this paper is available from the lead contact upon request.
- All other data reported in this paper will be shared by the lead contact upon request.

ACKNOWLEDGMENTS

Special thanks to all members of the Heller laboratory and Stanford OHNS Department for insightful discussions during the completion of this project. 10x Genomics single-cell RNA-seq was performed at the Stanford Functional Genomics Facility (S10OD025212 and 1S10OD021763). This project was supported by philanthropic donors to the Stanford Initiative to Cure Hearing Loss, as well as by the Stanford School of Medicine OHNS Clinician-Scientist Training Program in Otolaryngology T32 DC015209 (to M.S.M), Stanford School of Medicine Dean's Postdoctoral Fellowship (to M.S.M.), American Association of University Women (AAUW) American Fellowship (to M.S.M.), NIH K99 DC021984 (to M.S.M.), and NIH R21 DC019910 (to S.H.).

AUTHOR CONTRIBUTIONS

Conceptualization, M.S.M. and S.H.; methodology, M.S.M.; formal analysis, M.S.M.; investigation, M.S.M.; visualization, M.S.M.; funding acquisition, M.S.M. and S.H.; project administration, S.H.; supervision, S.H.; writing—original draft, M.S.M. and S.H.; writing—review and editing, M.S.M. and S.H.

DECLARATION OF INTERESTS

The authors declare no competing interests.

STAR★METHODS

Detailed methods are provided in the online version of this paper and include the following:

- KEY RESOURCES TABLE
- EXPERIMENTAL MODEL AND STUDY PARTICIPANT DETAILS
  - mESC culture and generation of inner ear organoids
- METHOD DETAILS
  - Single-cell RNA sequencing and data analysis
  - Quantitative PCR
  - Immunohistochemistry
  - EdU assay
- QUANTIFICATION AND STATISTICAL ANALYSIS

SUPPLEMENTAL INFORMATION

Supplemental information can be found online at https://doi.org/10.1016/j.isci.2025.111817.

Received: July 12, 2024
Revised: October 16, 2024
Accepted: January 13, 2025
Published: January 16, 2025

REFERENCES

1. Schlosser, G. (2014). Early embryonic specification of vertebrate cranial placodes. WIREs Dev. Biol. *3*, 349–363. https://doi.org/10.1002/wdev.142.
2. Heydari, Z., Moeinvaziri, F., Agarwal, T., Pooyan, P., Shpichka, A., Maiti, T.K., Timashev, P., Baharvand, H., and Vosough, M. (2021). Organoids: a novel modality in disease modeling. Biodes. Manuf. *4*, 689–716. https://doi.org/10.1007/s42242-021-00150-7.
3. DeJonge, R.E., Liu, X.P., Deig, C.R., Heller, S., Koehler, K.R., and Hashino, E. (2016). Modulation of Wnt signaling enhances inner ear organoid development in 3D culture. PLoS One *11*, e0162508. https://doi.org/10.1371/journal.pone.0162508.
4. Janesick, A., Hashino, E., and Heller, S. (2023). Inner Ear Cells from Stem Cells: A Path Towards Inner Ear Cell Regeneration. In Springer Handbook of Auditory Research: Hair Cell Regeneration (Springer), pp. 135–162. https://doi.org/10.1007/978-3-031-20661-0_6.
5. Moore, S.T., Nakamura, T., Nie, J., Solivais, A.J., Aristizábal-Ramírez, I., Ueda, Y., Manikandan, M., Reddy, V.S., Romano, D.R., Hoffman, J.R., et al. (2023). Generating high-fidelity cochlear organoids from human

pluripotent stem cells. Cell Stem Cell *30*, 950–961.e7. https://doi.org/10.1016/j.stem.2023.06.006.

6. Nie, J., Koehler, K.R., and Hashino, E. (2017). Directed Differentiation of Mouse Embryonic Stem Cells Into Inner Ear Sensory Epithelia in 3D Culture. Methods Mol. Biol. *1597*, 67–83. https://doi.org/10.1007/978-1-4939-6949-4_6.
7. Tang, P.C., Alex, A.L., Nie, J., Lee, J., Roth, A.A., Booth, K.T., Koehler, K.R., Hashino, E., and Nelson, R.F. (2019). Defective Tmprss3-Associated Hair Cell Degeneration in Inner Ear Organoids. Stem Cell Rep. *13*, 147–162. https://doi.org/10.1016/j.stemcr.2019.05.014.
8. Koehler, K.R., Mikosz, A.M., Molosh, A.I., Patel, D., and Hashino, E. (2013). Generation of inner ear sensory epithelia from pluripotent stem cells in 3D culture. Nature *500*, 217–221. https://doi.org/10.1038/nature12298.
9. Koehler, K.R., and Hashino, E. (2014). Three-dimensional mouse embryonic stem cell culture for generating inner ear organoids. Nat. Protoc. *9*, 1229–1244. https://doi.org/10.1038/nprot.2014.100.
10. Zhu, Q., Song, L., Peng, G., Sun, N., Chen, J., Zhang, T., Sheng, N., Tang, W., Qian, C., Qiao, Y., et al. (2014). The transcription factor Pou3f1 promotes neural fate commitment via activation of neural lineage genes and inhibition of external signaling pathways. Elife *3*, e02224. https://doi.org/10.7554/eLife.02224.
11. Kuang, Y.L., Munoz, A., Nalula, G., Santostefano, K.E., Sanghez, V., Sanchez, G., Terada, N., Mattis, A.N., Iacovino, M., Iribarren, C., et al. (2019). Evaluation of commonly used ectoderm markers in iPSC trilineage differentiation. Stem Cell Res. *37*, 101434. https://doi.org/10.1016/j.scr.2019.101434.
12. Zhao, W., Ji, X., Zhang, F., Li, L., and Ma, L. (2012). Embryonic Stem Cell Markers. Molecules *17*, 6196–6236. https://doi.org/10.3390/molecules17066196.
13. Wen, J., Zeng, Y., Fang, Z., Gu, J., Ge, L., Tang, F., Qu, Z., Hu, J., Cui, Y., Zhang, K., et al. (2017). Single-cell analysis reveals lineage segregation in early post-implantation mouse embryos. J. Biol. Chem. *292*, 9840–9854. https://doi.org/10.1074/jbc.M117.780585.
14. Ealy, M., Ellwanger, D.C., Kosaric, N., Stapper, A.P., and Heller, S. (2016). Single-cell analysis delineates a trajectory toward the human early otic lineage. Proc. Natl. Acad. Sci. USA *113*, 8508–8513. https://doi.org/10.1073/pnas.1605537113.
15. Efroni, S., Duttagupta, R., Cheng, J., Dehghani, H., Hoeppner, D.J., Dash, C., Bazett-Jones, D.P., Le Grice, S., McKay, R.D.G., Buetow, K.H., et al. (2008). Global Transcription in Pluripotent Embryonic Stem Cells. Cell Stem Cell *2*, 437–447. https://doi.org/10.1016/j.stem.2008.03.021.
16. Kurtz, A., Zimmer, A., Schnütgen, F., Brüning, G., Spener, F., and Müller, T. (1994). The expression pattern of a novel gene encoding brain-fatty acid binding protein correlates with neuronal and glial cell development. Development *120*, 2637–2649. https://doi.org/10.1242/dev.120.9.2637.
17. Matern, M.S., Durruthy-Durruthy, R., Birol, O., Darmanis, S., Scheibinger, M., Groves, A.K., and Heller, S. (2023). Transcriptional dynamics of delaminating neuroblasts in the mouse otic vesicle. Cell Rep. *42*, 112545. https://doi.org/10.1016/j.celrep.2023.112545.
18. Steinhart, M.R., van der Valk, W.H., Osorio, D., Serdy, S.A., Zhang, J., Nist-Lund, C., Kim, J., Moncada-Reid, C., Sun, L., Lee, J., and Koehler, K.R. (2023). Mapping oto-pharyngeal development in a human inner ear organoid model. Development *150*, dev201871. https://doi.org/10.1242/dev.201871.
19. Rose, K.P., Manilla, G., Milon, B., Zalzman, O., Song, Y., Coate, T.M., and Hertzano, R. (2023). Spatially distinct otic mesenchyme cells show molecular and functional heterogeneity patterns before hearing onset. iScience *26*, 107769. https://doi.org/10.1016/j.isci.2023.107769.
20. Hartman, B.H., Durruthy-Durruthy, R., Laske, R.D., Losorelli, S., and Heller, S. (2015). Identification and characterization of mouse otic sensory lineage genes. Front. Cell. Neurosci. *9*, 79. https://doi.org/10.3389/fncel.2015.00079.
21. Durruthy-Durruthy, R., Gottlieb, A., Hartman, B.H., Waldhaus, J., Laske, R.D., Altman, R., and Heller, S. (2014). Reconstruction of the Mouse Otocyst and Early Neuroblast Lineage at Single Cell Resolution. Cell *157*, 964–978. https://doi.org/10.1016/j.cell.2014.03.036.
22. Wu, D.K., and Kelley, M.W. (2012). Molecular Mechanisms of Inner Ear Development. Cold Spring Harb. Perspect. Biol. *4*, a008409. https://doi.org/10.1101/cshperspect.a008409.
23. Sun, Y., Wang, L., Zhu, T., Wu, B., Wang, G., Luo, Z., Li, C., Wei, W., and Liu, Z. (2022). Single-cell transcriptomic landscapes of the otic neuronal lineage at multiple early embryonic ages. Cell Rep. *38*, 110542. https://doi.org/10.1016/j.celrep.2022.110542.
24. Vu, T.H., Takechi, M., Shimizu, M., Kitazawa, T., Higashiyama, H., Iwase, A., Kurihara, H., and Iseki, S. (2021). Dlx5-augmentation in neural crest cells reveals early development and differentiation potential of mouse apical head mesenchyme. Sci. Rep. *11*, 2092. https://doi.org/10.1038/s41598-021-81434-x.
25. Guo, S., Zhang, Y., Zhou, T., Wang, D., Weng, Y., Chen, Q., Ma, J., Li, Y.P., and Wang, L. (2018). GATA4 as a novel regulator involved in the development of the neural crest and craniofacial skeleton via Barx1. Cell Death Differ. *25*, 1996–2009. https://doi.org/10.1038/s41418-018-0083-x.
26. Matern, M.S., Milon, B., Lipford, E.L., McMurray, M., Ogawa, Y., Tkaczuk, A., Song, Y., Elkon, R., and Hertzano, R. (2020). GFI1 functions to repress neuronal gene expression in the developing inner ear hair cells. Development *147*, dev186015. https://doi.org/10.1242/dev.186015.
27. Yu, H.V., Tao, L., Llamas, J., Wang, X., Nguyen, J.D., Trecek, T., and Segil, N. (2021). POU4F3 pioneer activity enables ATOH1 to drive diverse mechanoreceptor differentiation through a feed-forward epigenetic mechanism. Proc. Natl. Acad. Sci. USA *118*, e2105137118. https://doi.org/10.1073/pnas.2105137118.
28. Oshima, K., Shin, K., Diensthuber, M., Peng, A.W., Ricci, A.J., and Heller, S. (2010). Mechanosensitive Hair Cell-Like Cells from Embryonic and Induced Pluripotent Stem Cells. Cell *141*, 704–716. https://doi.org/10.1016/j.cell.2010.03.035.
29. Adhikari, A., Kim, W., and Davie, J. (2021). Myogenin is required for assembly of the transcription machinery on muscle genes during skeletal muscle differentiation. PLoS One *16*, e0245618. https://doi.org/10.1371/journal.pone.0245618.
30. Hartman, B.H., Böscke, R., Ellwanger, D.C., Keymeulen, S., Scheibinger, M., and Heller, S. (2018). Fbxo2VHC mouse and embryonic stem cell reporter lines delineate *in vitro*-generated inner ear sensory epithelia cells and enable otic lineage selection and Cre-recombination. Dev. Biol. *443*, 64–77. https://doi.org/10.1016/j.ydbio.2018.08.013.
31. Hao, Y., Hao, S., Andersen-Nissen, E., Mauck, W.M., Zheng, S., Butler, A., Lee, M.J., Wilk, A.J., Darby, C., Zager, M., et al. (2021). Integrated analysis of multimodal single-cell data. Cell *184*, 3573–3587.e29. https://doi.org/10.1016/j.cell.2021.04.048.
32. Wu, Y., Tamayo, P., and Zhang, K. (2018). Visualizing and Interpreting Single-Cell Gene Expression Datasets with Similarity Weighted Nonnegative Embedding. Cell Syst. *7*, 656–666.e4. https://doi.org/10.1016/j.cels.2018.10.015.
33. Rose, M.F., Ren, J., Ahmad, K.A., Chao, H.T., Klisch, T.J., Flora, A., Greer, J.J., and Zoghbi, H.Y. (2009). Math1 is essential for the development of hindbrain neurons critical for perinatal breathing. Neuron *64*, 341–354. https://doi.org/10.1016/j.neuron.2009.10.023.
34. Wiwatpanit, T., Lorenzen, S.M., Cantú, J.A., Foo, C.Z., Hogan, A.K., Márquez, F., Clancy, J.C., Schipma, M.J., Cheatham, M.A., Duggan, A., and García-Añoveros, J. (2018). Trans-differentiation of outer hair cells into inner hair cells in the absence of INSM1. Nature *1*, 1. https://doi.org/10.1038/s41586-018-0570-8.
35. Lorenzen, S.M., Duggan, A., Osipovich, A.B., Magnuson, M.A., and García-Añoveros, J. (2015). Insm1 promotes neurogenic proliferation in delaminated otic progenitors. Mech. Dev. *138*, 233–245. https://doi.org/10.1016/j.mod.2015.11.001.

36. Jahan, I., Pan, N., Kersigo, J., and Fritzsch, B. (2013). Beyond generalized hair cells: molecular cues for hair cell types. Hear. Res. *297*, 30–41. https://doi.org/10.1016/j.heares.2012.11.008.

37. Jan, T.A., Eltawil, Y., Ling, A.H., Chen, L., Ellwanger, D.C., Heller, S., and Cheng, A.G. (2021). Spatiotemporal dynamics of inner ear sensory and non-sensory cells revealed by single-cell transcriptomics. Cell Rep. *36*, 109358. https://doi.org/10.1016/j.celrep.2021.109358.

38. Doda, D., Jimenez, S.A., Rehrauer, H., Carrenõ, J.F., Valsamides, V., Di Santo, S., Widmer, H.R., Edge, A., Locher, H., van der Valk, W.H., and Zhang, J. (2023). Human pluripotent stem cell-derived inner ear organoids recapitulate otic development *in vitro*. Development *150*, 1. https://doi.org/10.1242/dev.201865.

39. Whitfield, M.L., George, L.K., Grant, G.D., and Perou, C.M. (2006). Common markers of proliferation. Nat. Rev. Cancer *6*, 99–106. https://doi.org/10.1038/nrc1802.

40. Gnedeva, K., and Hudspeth, A.J. (2015). SoxC transcription factors are essential for the development of the inner ear. Proc. Natl. Acad. Sci. USA *112*, 14066–14071. https://doi.org/10.1073/pnas.1517371112.

41. Street, K., Risso, D., Fletcher, R.B., Das, D., Ngai, J., Yosef, N., Purdom, E., and Dudoit, S. (2018). Slingshot: Cell lineage and pseudotime inference for single-cell transcriptomics. BMC Genom. *19*, 477. https://doi.org/10.1186/s12864-018-4772-0.

42. Van den Berge, K., Roux de Bézieux, H., Street, K., Saelens, W., Cannoodt, R., Saeys, Y., Dudoit, S., and Clement, L. (2020). Trajectory-based differential expression analysis for single-cell sequencing data. Nat. Commun. *11*, 1–13. https://doi.org/10.1038/s41467-020-14766-3.

43. Nist-Lund, C.A., Pan, B., Patterson, A., Asai, Y., Chen, T., Zhou, W., Zhu, H., Romero, S., Resnik, J., Polley, D.B., et al. (2019). Improved TMC1 gene therapy restores hearing and balance in mice with genetic inner ear disorders. Nat. Commun. *10*, 236. https://doi.org/10.1038/s41467-018-08264-w.

44. He, D., Guo, R., Zheng, D., Xu, M., Li, P., Guo, L., and Gan, L. (2020). Transcription factor Isl1 is dispensable for the development of the mouse prosensory region. Cytotechnology *72*, 407–414. https://doi.org/10.1007/s10616-020-00387-7.

45. Brown, R., and Groves, A.K. (2020). Hear, hear for notch: Control of cell fates in the inner ear by notch signaling. Biomolecules *10*, 370. https://doi.org/10.3390/biom10030370.

46. Zallocchi, M., Meehan, D.T., Delimont, D., Askew, C., Garige, S., Gratton, M.A., Rothermund-Franklin, C.A., and Cosgrove, D. (2009). Localization and expression of clarin-1, the Clrn1 gene product, in auditory hair cells and photoreceptors. Hear. Res. *255*, 109–120. https://doi.org/10.1016/j.heares.2009.06.006.

47. Liu, X.Z., Walsh, J., Mburu, P., Kendrick-Jones, J., Cope, M.J., Steel, K.P., and Brown, S.D. (1997). Mutations in the myosin VIIA gene cause non-syndromic recessive deafness. Nat. Genet. *16*, 188–190. https://doi.org/10.1038/ng0697-188.

48. Ruel, J., Emery, S., Nouvian, R., Bersot, T., Amilhon, B., Van Rybroek, J.M., Rebillard, G., Lenoir, M., Eybalin, M., Delprat, B., et al. (2008). Impairment of SLC17A8 encoding vesicular glutamate transporter-3, VGLUT3, underlies nonsyndromic deafness DFNA25 and inner hair cell dysfunction in null mice. Am. J. Hum. Genet. *83*, 278–292. https://doi.org/10.1016/j.ajhg.2008.07.008.

49. Yasunaga, S., Grati, M., Cohen-Salmon, M., El-Amraoui, A., Mustapha, M., Salem, N., El-Zir, E., Loiselet, J., and Petit, C. (1999). A mutation in OTOF, encoding otoferlin, a FER-1-like protein, causes DFNB9, a nonsyndromic form of deafness. Nat. Genet. *21*, 363–369. https://doi.org/10.1038/7693.

50. Chen, P., and Segil, N. (1999). p27(Kip1) links cell proliferation to morphogenesis in the developing organ of Corti. Development *126*, 1581–1590. https://doi.org/10.1242/dev.126.8.1581.

51. Kazmierczak, P., Sakaguchi, H., Tokita, J., Wilson-Kubalek, E.M., Milligan, R.A., Müller, U., and Kachar, B. (2007). Cadherin 23 and protocadherin 15 interact to form tip-link filaments in sensory hair cells. Nature *449*, 87–91. https://doi.org/10.1038/nature06091.

52. McInturff, S., Burns, J.C., and Kelley, M.W. (2018). Characterization of spatial and temporal development of Type I and Type II hair cells in the mouse utricle using new cell-type-specific markers. Biol. Open *7*, bio038083. https://doi.org/10.1242/bio.038083.

53. Liu, X.P., Koehler, K.R., Mikosz, A.M., Hashino, E., and Holt, J.R. (2016). Functional development of mechanosensitive hair cells in stem cell-derived organoids parallels native vestibular hair cells. Nat. Commun. *7*, 11508. https://doi.org/10.1038/ncomms11508.

54. Koehler, K.R., Nie, J., Longworth-Mills, E., Liu, X.P., Lee, J., Holt, J.R., and Hashino, E. (2017). Generation of inner ear organoids with functional hair cells from human pluripotent stem cells. Nat. Biotechnol. *35*, 583–589. https://doi.org/10.1038/nbt.3840.

55. Ueda, Y., Nakamura, T., Nie, J., Solivais, A.J., Hoffman, J.R., Daye, B.J., and Hashino, E. (2023). Defining developmental trajectories of prosensory cells in human inner ear organoids at single-cell resolution. Development *150*, dev201071. https://doi.org/10.1242/dev.201071.

56. van der Valk, W.H., van Beelen, E.S.A., Steinhart, M.R., Nist-Lund, C., Osorio, D., de Groot, J.C.M.J., Sun, L., van Benthem, P.P.G., Koehler, K.R., and Locher, H. (2023). A single-cell level comparison of human inner ear organoids with the human cochlea and vestibular organs. Cell Rep. *42*, 112623. https://doi.org/10.1016/j.celrep.2023.112623.

57. Waldhaus, J., Jiang, L., Liu, L., Liu, J., and Duncan, R.K. (2024). Mapping the developmental potential of mouse inner ear organoids at single-cell resolution. iScience *27*, 109069. https://doi.org/10.1016/j.isci.2024.109069.

58. Perny, M., Ting, C.C., Kleinlogel, S., Senn, P., and Roccio, M. (2017). Generation of Otic Sensory Neurons from Mouse Embryonic Stem Cells in 3D Culture. Front. Cell. Neurosci. *11*, 409. https://doi.org/10.3389/fncel.2017.00409.

59. Orvis, J., Gottfried, B., Kancherla, J., Adkins, R.S., Song, Y., Dror, A.A., Olley, D., Rose, K., Chrysostomou, E., Kelly, M.C., et al. (2021). gEAR: Gene Expression Analysis Resource portal for community-driven, multi-omic data exploration. Nat. Methods *18*, 843–844. https://doi.org/10.1038/s41592-021-01200-9.

60. Zheng, G.X.Y., Terry, J.M., Belgrader, P., Ryvkin, P., Bent, Z.W., Wilson, R., Ziraldo, S.B., Wheeler, T.D., McDermott, G.P., Zhu, J., et al. (2017). Massively parallel digital transcriptional profiling of single cells. Nat. Commun. *8*, 14049. https://doi.org/10.1038/ncomms14049.

61. Haghverdi, L., Lun, A.T.L., Morgan, M.D., and Marioni, J.C. (2018). Batch effects in single-cell RNA sequencing data are corrected by matching mutual nearest neighbours. Nat. Biotechnol. *36*, 421–427. https://doi.org/10.1038/nbt.4091.

62. Marsh, S. (2024). scCustomize: Custom Visualizations & Functions for Streamlined Analyses of Single Cell Sequencing. https://doi.org/10.32614/CRAN.package.scCustomize.

63. Ge, S.X., Jung, D., and Yao, R. (2020). ShinyGO: a graphical gene-set enrichment tool for animals and plants. Bioinformatics *36*, 2628–2629. https://doi.org/10.1093/bioinformatics/btz931.

STAR★METHODS

KEY RESOURCES TABLE

REAGENT or RESOURCE	SOURCE	IDENTIFIER
Antibodies		
mouse anti-Ecad	Fisher Scientific	RRID:AB_397580
goat anti-Sox2	Santa Cruz	RRID:AB_2286684
rabbit anti-Pax8	Abcam	RRID:AB_10679472
rabbit anti-Myo7a	Proteus	RRID:AB_10015251
goat anti-Jag1	Santa Cruz	RRID:AB_649689
rabbit anti-Oct4	Life Technologies	RRID:AB_3074191
rabbit anti-Twist1/2	GeneTex	RRID:AB_2885640
mouse anti-Tubb3	Biolegend	RRID:AB_2313773
rabbit anti-Neurod1	Proteintech	RRID:AB_2877823
mouse anti-P63	Biocare Medical	RRID:AB_10582730
rat anti-Epcam-APC	BioLegend	RRID:AB_1134102
rabbit anti-Pou3f4	ProteinTech	RRID:AB_2879903
rabbit anti-Fabp7	Abcam	RRID:AB_880078
rabbit anti-Phox2b	ThermoFisher	RRID:AB_2880001
mouse anti-Pou4f3	Santa Cruz	RRID:AB_2167543
mouse anti-Calb2	Millipore Sigma	RRID:AB_94259
rabbit anti-Pvalb	Author generated	NA
mouse anti-Otof	Abcam	RRID:AB_881807
rat anti-Ki67	ThermoFisher	RRID:AB_10853185
mouse anti-p27kip1	ThermoFisher	Cat#1027-MSM3-P0; RRID:AB_1931933
mouse anti-Spp1	Biotechne R&D systems	RRID:AB_2194992
donkey anti-mouse Alexa Fluor 488	ThermoFisher	RRID:AB_141607
donkey anti-rabbit Alexa Fluor 546	ThermoFisher	RRID:AB_2534016
donkey anti-goat Alexa Fluor 647	ThermoFisher	RRID:AB_2535864
donkey anti-rat Alexa Fluor 488	ThermoFisher	RRID:AB_2535794
donkey anti-rat Alexa Fluor 647	ThermoFisher	RRID:AB_2893138
donkey anti-mouse Alexa Fluor 546	ThermoFisher	RRID:AB_11180613
donkey anti-goat Alexa Fluor 488	ThermoFisher	RRID:AB_2534102
Chemicals, peptides, and recombinant proteins		
EmbryoMax 0.1% Gelatin Solution	Millipore Sigma	Cat#ES-006-B
ESGRO Leukemia Inhibitory Factor (LIF)	Sigma	Cat#ESG1106
Mirdametinib (PD0325901)	Selleckchem	Cat#S1036
CHIR-99021 (CT99021) HCl	Selleckchem	Cat#S2924
Stemfactor BMP-4, Human Recombinant	Reprocell	Cat#03-0007
RepSox	Selleckchem	Cat#S7223
Recombinant Human FGF-basic (154 a.a.)	Peprotech	Cat#100-18B
Stemolecule™ LDN-193189	Reprocell	Cat#04-0074-02
EdU (5-ethynyl-2'-deoxyuridine)	Santa Cruz	Cat#sc-284628A
DAPI	Thermo Fisher Scientific	Cat#D1306
Alexa Fluor 488 phalloidin	Invitrogen	Cat#A-12379
Accutase	Innovative Cell Technologies, Inc	Cat#AT104
Thermolysin	Sigma	Cat#P1512
Paraformaldehyde	EMS	Cat#15710

(*Continued on next page*)

Continued		
REAGENT or RESOURCE	SOURCE	IDENTIFIER
Critical commercial assays		
Click-iT EdU Cell Proliferation Kit	Thermo Fisher	Cat#C10340
Deposited data		
scRNA-seq of DIV3, DIV4, DIV8, DIV11, DIV16 and DIV21 mESC-derived organoids	This paper	GEO: GSE252570
Seurat objects for scRNA-seq data analyses	This paper	Mendeley Data: https://doi.org/10.17632/tgsssyzwwg.1
Experimental models: Cell lines		
Fbxo2-VHC mESCs	Hartman et al.[30]	NA
Atoh1/nGFP mESCs	Oshima et al.[28]	NA
Oligonucleotides		
Primers for qPCR	This paper	Data S4
Software and algorithms		
R	R Project for Statistical Computing	RRID:SCR_001905
Cell Ranger	10x Genomics, Zheng et al.[60]	RRID:SCR_017344
RStudio	https://www.rstudio.com/	Version 2023.03.0+386
Seurat	https://cran.r-project.org/web/packages/Seurat/	RRID:SCR_016341
swne	Wu et al.[32]	Version 0.6.20
Slingshot	Street et al.[41]	RRID:SCR_017012
tradeSeq	Van den Berge et al.[42]	RRID:SCR_019238
pheatmap	https://www.rdocumentation.org/packages/pheatmap	RRID:SCR_016418
batchelor	Haghverdi et al.[61]	Version 1.14.1
scCustomize	https://samuel-marsh.github.io/scCustomize/	RRID:SCR_024675
Inkscape	https://inkscape.org/	RRID:SCR_014479
Fiji/ImageJ	https://fiji.sc	RRID:SCR_002285
ShinyGO	http://bioinformatics.sdstate.edu/go/	RRID:SCR_019213

EXPERIMENTAL MODEL AND STUDY PARTICIPANT DETAILS

mESC culture and generation of inner ear organoids

Fbxo2-VHC[30] and *Atoh1*/nGFP[28] mESCs were maintained without feeder cells on 0.1% gelatin (Millipore) coated plates in 2iLIF media (N2/B27 supplemented with 1000 units/mL recombinant mouse LIF protein (ESGRO), 1 μM MEK inhibitor PD0325901 (Selleckchem) and 3 μM Wnt activator CHIR99021 (Selleckchem). Vestibular-like inner ear organoids were generated as previously described,[3,30,57] with minor modifications. Briefly, dissociated *Fbxo2-VHC* or *Atoh1*/nGFP mESCs were resuspended in ectodermal differentiation medium and plated into 96-well U-bottom suspension plates (Nunclon Sphera, Thermo Fisher) at a concentration of 3,000 cells per well. At day *in vitro* (DIV) 1, the media was supplemented with 2% matrigel (Corning). On DIV3, organoids were exposed to 10 ng/mL BMP4 (Reprocell) to induce BMP signaling and 1 μM RepSox (a TGFβRI inhibitor, Selleckchem) to repress TGFβ signaling. On DIV4, developing organoids were further exposed to 50 ng/mL FGF2 (Peprotech) to induce FGF signaling and 1 μM LDN193189 (an inhibitor of BMP type I receptors, Reprocell) to repress BMP signaling. On DIV8, organoids were washed with 1X PBS and transferred to maturation media containing 1% matrigel and 3 μM CHIR99021 (a GSK-3α/β inhibitor, Selleckchem) to induce Wnt signaling. After DIV10, half of the media was changed every 2-3 days until the last time point at DIV21.

METHOD DETAILS

Single-cell RNA sequencing and data analysis

For DIV3 and DIV4 time points, organoids were washed once in 1X PBS, incubated in Accutase dissociation reagent (Invitrogen) for 3 minutes at 37°C, and dissociated by manual trituration with a P200 pipette tip. Incubation and trituration were repeated twice. DIV8, DIV11, DIV16, and DIV21 organoids were first incubated for 20 minutes in 0.5 mg/mL Thermolysin (Promega) at 37°C before

incubation in Accutase (STEMCELL Technologies) for 3 minutes. Organoids were then mechanically dissociated using a 23G blunt-ended needle connected to a sterile 1 mL syringe, returned to the incubator for an additional 3 minutes, and dissociated a second time. Cells from all time points were then collected in 1 mL 1X PBS, spun down at 4°C at 400x g for 10 minutes, and resuspended in 400 μL of DMEM/F12 + 10% fetal bovine serum (FBS). Cell clumps were removed by filtering through a 35 μm strainer cap (Corning). Cells were then placed on ice and brought immediately to the Stanford Functional Genomics Facility for cell capture and processing using 10x Genomics Chromium Single Cell 3' Reagents v3.1. The resulting libraries were sequenced on a NovaSeq 6000 (Illumina) using a 150bp paired-end read configuration.

Reads were aligned to the mouse reference genome mm10 using 10x Genomics Cell Ranger v6.0.0 with default parameters.[60] The resulting filtered digital gene expression matrices were used for downstream data analysis using Seurat v4.3.0.[31] After filtering for high quality cells (number of features between 200 and 10000, total counts greater than 10000, and mitochondrial gene expression less than 5%), similar cell numbers were obtained for each time point with the exception of DIV4, which is represented by fewer cells that still aligned well with the preceding and subsequent time points. DIV11, 16, and 21 otic lineage cells were combined using the Seurat function IntegrateData and visualized with SWNE plots.[32] scCustomize was also used for data visualization and figure generation.[62] Trajectory analysis was performed using Slingshot with cluster SC-4 set as the starting cluster and extend = "n". Significantly changed genes along the identified trajectories (FDR <0.05) were calculated using the tradeSeq function associationTest with lineages = T.[41,42] Gene ontology analysis of pseudotime gene clusters was performed using ShinyGo v0.80.[63] DIV11, 16, and 21 organoid hair cell profiles were combined with utricle hair cell profiles using batchelor and analyzed using Seurat.[37,52,61]

Quantitative PCR

Total RNA from whole organoids was extracted using the Direct-zol RNA Miniprep kit (Zymo Research) and cDNA was generated using the Maxima First Strand cDNA Synthesis Kit for RT-qPCR (Thermo Fisher). RT-qPCR was performed using Maxima SYBR Green/ROX qPCR Master Mix (Thermo Fisher). Primers are listed in Data S4.

Immunohistochemistry

Inner ear organoids were collected and washed once with 1X PBS before fixation in 4% paraformaldehyde (PFA) in 1X PBS overnight at 4°C. Fixed organoids were then embedded in 5% Certified Low Melt Agarose (BioRad) in 1X PBS and sectioned to 100 μm using a Leica VT1200 vibratome (1 mm amplitude, 0.8 mm/sec speed). Organoid sections were punched out using a 2 mm Acu-Punch Disposable Biopsy Punch (Acuderm Inc) and transferred into cut 35 μm cell strainer lids (Corning) within 48-well plates for immunostaining. Primary antibodies are listed in Data S4. Complementary Alexa Fluor 647, 546, and 488 labeled antibodies (1:1000, Invitrogen) were used for secondary detection. F-actin was stained using Alexa Fluor 488 phalloidin (1:200, Invitrogen), and cell nuclei were stained with DAPI (25 μg/ml, Invitrogen). Sections were mounted in FluorSave Reagent (EMD Millipore) within 13 mm diameter, 0.12 mm deep Secure-Seal Spacers (Thermo Fisher) adhered to specimen slides. Images were acquired at the Stanford OHNS Imaging Core Facility using either a Zeiss LSM700 or LSM880 confocal microscope and Zen Black software (Zeiss). FIJI (ImageJ, NIH) was used for image processing.

EdU assay

Sterile filtered EdU (Thermo Fisher) in DMSO was added to organoid culture media to a final concentration of 10 μM at DIV10. After 2 hours, the EdU-containing media was removed, organoids were washed once in 1X PBS, and fresh media was added. 22 hours following EdU removal, organoids were collected and processed for vibratome sections as described. EdU integration was assessed using the Click-iT EdU Cell Proliferation Kit (Thermo Fisher) followed by primary and secondary antibody detection.

QUANTIFICATION AND STATISTICAL ANALYSIS

For RT-qPCR, data were analyzed using the ΔΔCt method, using *Actb* expression as the endogenous control. Statistical significance between samples was assessed by 2-way ANOVA followed by Tukey's multiple comparisons test in Prism 10 (GraphPad). For Ki67+ and $P27^{kip1}$+ otic cell quantification at DIV11, DIV16 and DIV21, the boundaries of otic regions were defined by SOX2 expression. Ki67+ and $P27^{kip1}$+ cells were counted using the Cell Counter plugin in FIJI and normalized to the total number of cells within the otic regions (DAPI+). Statistical significance between time points was assessed by ordinary one-way ANOVA followed by Tukey's multiple comparisons test in Prism 10 (GraphPad). Statistical details of experiments can be found in the corresponding figure legends. All experiments were performed in at least biological triplicate, with each biological replicate consisting of multiple organoids from a single batch.